



Effective combination of liposome-targeted chemotherapy and PD-L1 blockade of murine colon cancer

Zili Gu^a, Candido G. Da Silva^a, Yang Hao^a, Timo Schomann^{a,b}, Marcel G.M. Camps^c, K. van der Maaden^c, Qi Liu^d, Ferry Ossendorp^{c,*}, Luis J. Cruz^{a,*}

^a Department of Radiology, Leiden University Medical Center, the Netherlands

^b Percuros B.V., Leiden, the Netherlands

^c Department of Immunology, Leiden University Medical Center, the Netherlands

^d Department of Internal Medicine, University of Texas Southwestern Medical Center, Dallas, TX, USA

ARTICLE INFO

Keywords:

Liposomes
Nanomedicine
Chemoimmunotherapy
Checkpoint blockade

ABSTRACT

Therapeutic cancer drug efficacy can be limited by insufficient tumor penetration, rapid clearance, systemic toxicity and (acquired) drug resistance. The poor therapeutic index due to inefficient drug penetration and rapid drug clearance and toxicity can be improved by using a liposomal platform. Drug resistance for instance against pemetrexed, can be reduced by combination with docetaxel. Here, we developed a specific liposomal formulation to simultaneously deliver docetaxel and pemetrexed to enhance efficacy and safety. Hydrophobic docetaxel and hydrophilic pemetrexed were co-encapsulated into pH-sensitive liposomes using a thin-film hydration method with high efficiency. The physicochemical properties, toxicity, and immunological effects of liposomes were examined *in vitro*. Biodistribution, anti-tumor efficacy, and systemic immune response were evaluated *in vivo* in combination with PD-L1 immune checkpoint therapy using two murine colon cancer models. In cellular experiments, the liposomes exhibited strong cytotoxicity and induced immunogenic cell death. *In vivo*, the treatment with the liposome-based drug combination inhibited tumor development and stimulated immune responses. Liposomal encapsulation significantly reduced systemic toxicity compared to the delivery of the free drug. Tumor control was strongly enhanced when combined with anti-PD-L1 immunotherapy in immunocompetent mice carrying syngeneic MC38 or CT26 colon tumors. We showed that treatment with liposome-mediated chemotherapy of docetaxel and pemetrexed combined with anti-PD-L1 immunotherapy is a promising strategy for the treatment of colon cancers.

1. Introduction

The growing interest in combining various treatments for colorectal cancer is largely attributable to the vital significance to improve clinical outcomes for such cancer patients [1]. Chemotherapy, as well as surgery and radiotherapy, are currently the main strategies utilized for intervention of colorectal cancer [2]. Although chemotherapy is already widely used today, there are several restrictions, such as drug tolerance,

poor circulation *in vivo*, and systemic toxicity [3–5].

Pemetrexed (PMX) is a unique folate antagonist that inhibits multiple folate-metabolizing enzymes, causing an imbalance in the cellular nucleotide pool, interfering with DNA and RNA synthesis, and eventually leading to (cancer) cell death [6]. However, cancer cells eventually develop chemoresistance that hinders therapeutic efficacy after continuous exposure to PMX [7]. Previous studies have shown that, among the enzymes targeted by PMX, low levels of thymidylate synthase

Abbreviations: Adpgk, ADP-dependent Glucokinase; BSA, bovine serum albumin; CHEMS, cholestryl hemisuccinate; CryoEM, cryo-electron microscope; CRT, calreticulin; DCs, dendritic cells; DTX, docetaxel; DL, drug loading; DLS, dynamic light scattering; DOPE, dioleylphosphatidylamine; DTX-LP, docetaxel-loaded liposomes; DTX/PMX-LP, co-loaded liposomes; EE, encapsulation efficiency; HMGB1, High-mobility group box 1; ICD, immunogenic cell death; MHC, major histocompatibility complex; PMX, pemetrexed; IR780-LP, IR780-loaded liposomes; TEM, transmission electron microscopy; TS, thymidylate synthase; PEG, poly(ethyl glyco); PBS, Phosphate Buffered Saline; PDI, polydiverse index; PMX-LP, pemetrexed-loaded liposomes; PVDF, polyvinylidene fluoride; RCV, Relative cell viability; Rpl18, ribosomal protein L18; UPLC, ultra-high-performance liquid chromatography.

* Corresponding authors.

E-mail addresses: F.A.Ossendorp@lumc.nl (F. Ossendorp), l.j.cruz_ricondo@lumc.nl (L.J. Cruz).

<https://doi.org/10.1016/j.jconrel.2022.11.049>

Received 28 September 2022; Received in revised form 24 November 2022; Accepted 28 November 2022
0168-3659/© 2022 Published by Elsevier B.V.

(TS) expression are linked to PMX-based chemosensitivity—the stronger the expression of TS, the lower the sensitivity to PMX [8,9]. It has been shown that docetaxel (DTX) can activate wild-type tumor protein P53 to suppress TS expression, which leads to higher PMX sensitivity in non-small cell lung cancer²⁵. However, various limitations of chemotherapeutic agents can impair their bioavailability and ultimate therapeutic effects, including low penetration into tumor tissue, rapid clearance in blood, lack of selectivity, high adverse effects, etc. [10]. Therefore, it is necessary to choose a proper delivery system that offers advantages over standard formulations.

In the emerging field of nanomedicine, liposomes are used to improve pharmacological therapy and to provide novel modalities in disease prevention, diagnosis, and treatment [11,12]. They hold the potential to address the shortcomings associated with biologics and have distinctive features to deliver cargos to a selected cell type or organ [13]. Importantly, compared to free combination, loading cytotoxic agents into one liposome tends to exhibit higher biological effects. Liposomes also allow for the synchronization and regulation of pharmacokinetics and biodistribution, as well as uniform time and spatial co-delivery of two agents. To efficiently deliver drugs into tumor cells, a PEGylated pH-sensitive liposomal formulation co-loaded with DTX and PMX was designed and prepared. In these liposomes, dioleylphosphatidylamine (DOPE) is one of the key ingredients for pH sensitivity, which is mediated by the conversion of the polar head group of DOPE, triggering membrane destabilization in presence of an acidic pH, and fusion with endosomal membranes, thus leading to cytoplasmic delivery of their contents [14]. Meanwhile, cholesteryl hemisuccinate (CHEMS) is used to stabilize DOPE bilayers at physiological pH. CHEMS is able to interact with the lipids of the cell membrane and thereby facilitates the fusion of DOPE with the cell membrane [14]. In addition, the PEGylation of liposomes can protect drugs from being degraded in the blood circulation until they enter the tumor cells, to induce local cytotoxicity and/or other effects such as further immune activation.

Nevertheless, this combination of DTX and PMX might still be insufficient in practice. In the clinic, cancer treatment has evolved from the empirical use of cytotoxic therapies to a hallmark of personalized treatment, with subsets of patients being treated based on the genetic alterations of their tumor and the expression of specific immune suppressive ligands. Such markers can be indicative for the benefit that patients could obtain from targeted therapies or immune checkpoint blockers, respectively [15]. More findings reveal that immunotherapy has a significant impact on the prognoses of many cancers, and the specific anti-cancer immune responses can predict patient outcomes following cancer chemotherapy [16]. As one of the preliminary immune checkpoint pathways in the tumor microenvironment, the programmed cell death protein 1(PD-1) -PD1 ligand 1 (PD-L1) receptor-ligand pair facilitates the immunosuppressive environment. In this study, anti-PD-L1 was used to block this pathway for an efficient cancer immune control. In addition, appropriately designed and dosed chemotherapeutic agents can be effective against immune suppressed cancers [17]. One of the most common mechanisms by which chemotherapy boosts immunity against cancer is by inducing immunogenic cell death (ICD). The benefit of inducing ICD is that the debris of cancer cells may act as a “vaccine” and boost the immune system with a relatively low dose of a chemotherapeutic drug. Furthermore, it is widely accepted that some chemotherapies can be combined with immunotherapy *via* liposomes, and those combinations synergistically lead to an improved therapeutic outcome [2,18,19].

In this study, we report that liposome-mediated co-delivery can enhance the sensitivity of colon cancer to chemotherapeutics, elicit ICD, and further improve anti-PD-L1 immunotherapy *via* immune activation. We chose PD-L1 as a target not only because it is one of the most vital checkpoints, but also because it has been shown to increase anti-tumor activity and induce inflamed/immune activation when inhibited in combination with DTX or PMX [20,21]. A schematic illustration of the strategy is shown in Fig. 1. The PEGylated, pH-sensitive liposomes

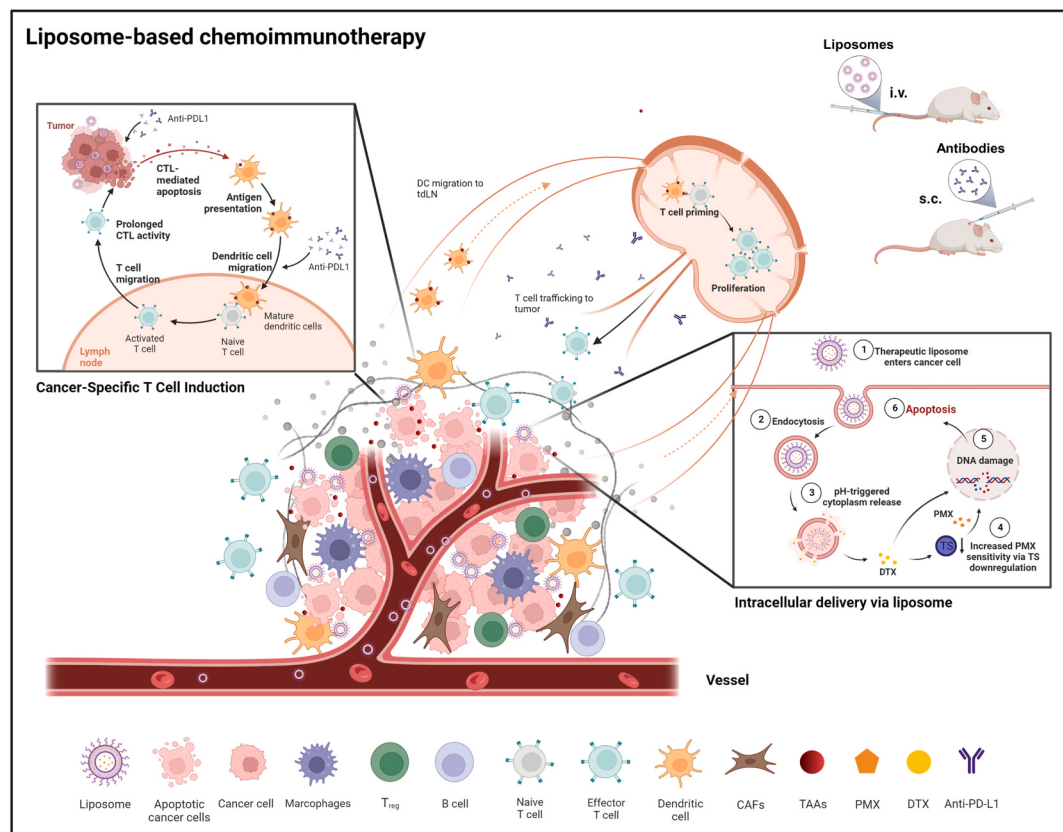


Fig. 1. Schematic illustration of chemoimmunotherapy by means of liposomal drug delivery.

accumulate in the tumor tissue after administration, followed by direct cell killing and strong induction of ICD. We could show that the therapeutic effect is improved since ICD enhances the immune activation and recruits more immune cells into the tumor tissue. Hence, our study reports the design a nano-platform to augment the anti-cancer effect of chemoimmunotherapy leading to efficient tumor control and improved survival.

2. Materials and methods

2.1. Materials

DOPE, Soy PC(SPC), CHEMS, Methoxy-polyethylene glycol (MW 2000)-distearoylphosphatidyl-ethanolamine (mPEG2000-DSPE) was purchased from Avanti Polar Lipids (Alabaster, USA). Chloroform (CHCl_3 MW 119.38 g/mol) was purchased from Merck (Darmstadt, Germany). The near infrared dye IR-780 (CAS 207399-07-3) was purchased from Sigma-Aldrich (Zwijndrecht, The Netherlands). DTX and PMX were purchased from MedChemExpress (NJ, USA).

2.2. Preparation of DTX/PMX-loaded liposomes

DTX and PMX were encapsulated into liposomes (defined as DTX/PMX-LPs) through mixing DOPE, SPC, CHEMS, and DSPE-PEG2000 (All from Avanti Polar Lipids, Alabaster, USA) at a specific molar ration using the thin-film hydration method [20]. Briefly, lipids are weighed and dissolved in chloroform at the indicated ratios (DOPE:SPC:CHEMS:DTX:DSPE-PEG200 = 1:1:1:0.08:0.04) and added to a round-bottomed flask. Chloroform was removed using a rotary evaporator (Rotavapor R-210, Büchi, Switzerland). The thin film generated was further dried under high vacuum for 2 h. The lipid film was then rehydrated with phosphate-buffered saline (PBS; pH 7.4) with PMX (4 mg/mL) at 40 °C for 0.5 h. The liposome dispersion was then placed in an Extruder (LIPEX Extruder, Northern Lipids Inc., Canada) and extruded through two stacked (400 nm and 100 nm) polycarbonate membrane filters (Whatman®, NucleporeTM, GE healthcare, Little Chalfont, UK) at least 6 times. After loading, free DTX and PMX were removed by Vivaspin2 (MWCO 100 kDa, Satorius, Göttingen, Germany) at room temperature. The final liposomes were collected and stored at 4 °C.

2.3. Characterization

A series of properties of these liposomes were evaluated including morphology observation, size distributions, zeta potentials, entrapment efficiency (EE %), and drug loading of DTX and PMX (DL %). The size and zeta potential of liposomes dispersed in 10 mM phosphate buffer were determined using dynamic light scattering (DLS) on a Zetasizer Nano S90 (Malvern Instruments, Malvern, London, UK). EE % and DL % of DTX and PMX were determined using ultra-high-performance liquid chromatography (UPLC; Waters, Milford, MA, USA) with a C18 column (ACQUITY, C18, 100 mm × 2.1 mm, 1.7 μm) at room temperature. Analytes were separated by a gradient elution and detected at 227 nm. A 10.0-fold amount of methanol was used to destroy the bilayer structure. The mobile phase was composed of A (0.1% v/v of trifluoroacetic acid in MQ) and B (0.1% v/v of trifluoroacetic acid in acetonitrile). The flow rate was 0.5 mL/min with a gradient program follows: 0–3 min 95% → 0% A, 3–5 min 0% A, 5–5.1 min 95% A, 5–8 min 95% A. The peak area connected with the standard curve was used to calculate the amount of DTX and PMX in the liposomes, respectively. Standard curves were created under the same conditions as those mentioned above. In the UPLC, all analyses were done in triplicate with a 10 μL injection volume. Drug encapsulation efficiency and loading efficiency were then calculated using the following equations:

$$\text{EE\%} = \frac{W_{\text{encapsulated drug}}}{W_{\text{total drug}}} \times 100\%$$

$$\text{DL\%} = \frac{W_{\text{encapsulated drug}}}{W_{\text{encapsulated drug}} + W_{\text{lipo}}} \times 100\%$$

where $W_{\text{encapsulated drug}}$ is the weight of drug encapsulated in liposomes; $W_{\text{total drug}}$ is the total weight of drug added; W_{lipo} is the weight of all the carrier materials in liposomes.

To visualize liposomes, transmission electron microscope (TEM) was used to examine the morphology of our liposomes. Briefly, 3 μL of sample solution were applied on the freshly glow-discharged grid and allowed to adhere for 1 min and then stained with 2% uranyl acetate in distilled water. After air-dried for 10 min, grids were examined using a Tecna 12 Twin (FEI Company, Hillsboro, Oregon, USA).

2.4. Stability and in-vitro release of co-loaded liposomes

To investigate the stability under different environments, liposomes were put in PBS and serum. The stability of our liposomes was assessed after storage at room temperature for 24 h. The mean vesicle size and zeta potential were measured using DLS. Furthermore, a dynamic dialysis method was used to assess the release behavior of DTX and PMX under different conditions of pH *in vitro*, as described below [22]. Different pH conditions were used to simulate the release behavior in blood circulation or lysosomes. A 1 mL aliquot of liposomes was transferred into dialysis tubing and placed in temperature-controlled, jacketed beaker containing 50 mL of 0.5% Tween in PBS at 37 °C. At indicated time intervals, samples were withdrawn from the release medium and assayed for DTX and PMX by UPLC as previously described [23,24].

2.5. Cell lines and cell culture

Murine MC-38 and CT-26 colon carcinoma cell lines were grown in full Iscove's Modified Dulbecco's Medium (IMDM; Lonza, Walkersville, MD, USA) supplemented with 10% heat-inactivated fetal calf serum (FCS, Sigma-Aldrich), 2 mM L-glutamine (Invitrogen, Waltham, MA, USA), 25 mM β-mercaptoethanol (Sigma-Aldrich), and 100 IU/ml penicillin/streptomycin (Gibco, Paisley, UK) at 37 °C and 5% CO₂ in an incubator (Panasonic). All cells were tested for mycoplasma and mouse antibody production (MAP) before use.

2.6. Animals

Female C57BL/6 and BALB/c mice were purchased from ENVIGO, and housed in pathogen-free animal facilities at Leiden University Medical Center (LUMC). All experimental animals were 6–8-weeks old unless otherwise stated. The animal experiments were designed according to the guidelines of the Dutch Animal Ethics Committee's Code of Conduct, with a project license AVD116008045, and strictly conducted according to the Dutch animal welfare law.

2.7. Investigation of PD-L1 expression level

To evaluate the PD-L1 expression levels of MC38 and CT26 colon tumor cell lines, 100,000 cells were resuspended in FACS buffer (PBS containing 0.5% bovine serum albumin and 0.1% NaN₃). Next, cells were incubated with PE-labeled CD44 (Clone IM7, Thermo Fisher Scientific, Waltham, MA, USA) and FITC-labeled PD-L1 (Clone MIH5, Thermo Fisher) at 4 °C for 30 min. These samples were washed three times with cold FACS buffer. The fluorescence signal was read using a flow cytometer (LSR II, BD bioscience, USA) and analysis was carried out using FlowJo (version 10).

2.8. Evaluation of cellular uptake and retention

As a lipophilic dye, IR780 (Sigma-Aldrich, St. Louis, MO, USA) was used to analyze cellular drug uptake as a substitution for DTX. 5×10^4

and 3×10^4 MC38 and CT26 cells were seeded in 24-well plate with coverslips. After incubation with free IR780 and IR780-loaded liposomes (IR780-LPs) for a specific duration, cells were quantitatively analyzed by means of flow cytometry (LSR II, BD bioscience). Meanwhile, immunofluorescence staining was performed for visualization. The cells were washed with PBS three times to remove extra liposomes or dye and fixed with 4% formaldehyde in PBS, followed by staining with anti-CD44-PE for 30 min and DAPI (Invitrogen) for 5 min. Confocal laser scanning microscopy (Leica SP5, Wetzlar, Germany) was used to observe the intracellular drug distribution.

2.9. Cytotoxicity assay of liposomal formulations *in vitro*

To explore the toxicity of nano-formulations, an MTS assay (CellTiter 96®, Promega, Madison, WI, USA) was used to measure the cell viability at different time points and concentrations. Therefore, 5000 and 3500 MC38 and CT26 cells were seeded per well of 96-well plates and incubated overnight. Various formulations were then added into each well at the designated concentration. After the incubation with MTS solution, the maximum absorbance was set at 490 nm and the optical density of each well was scanned on a microplate reader. Relative cell viability (RCV; %) was calculated as follows:

$$RCV (\%) = \frac{OD_{test} - OD_{blank}}{OD_{control} - OD_{blank}} \times 100\%$$

where OD_{blank} represents medium-filled wells, which did not contain any cells, OD_{test} and OD_{control} represent the OD of cells treated with our (nano-)formulations as well as the untreated control group, respectively.

Additionally, we investigated the apoptosis-inducing properties of our formulations *in vitro* by means of flow cytometry using an Annexin V-PI staining (Invitrogen), since DTX interferes with DNA replication and cell division during mitosis. The damaged DNA elicits DNA repair mechanisms, which in turn activate apoptosis when repair proves impossible.

2.10. Protein extraction and western blot analysis

Cell lysate was collected from cell cultures by adding pre-cold RIPA buffer before scraping adherent cells off the dishes. After centrifugation, lysates were aspirated from the tubes. Proteins (~20 µg) were added into gels for electrophoresis and transferred onto polyvinylidene fluoride (PVDF) membranes, which were previously incubated with polyclonal anti-TS (Cell Signaling Technology, Danvers, Massachusetts, USA) and anti-β-actin (Biologen, San Diego, CA, USA) separately. Next, anti-rabbit (Biologen) or anti-mouse (Biologen) IgG were conjugated to horseradish peroxidase. Pierce Fast Western Blot kit (Thermo Fisher Scientific) was used to detect the chemiluminescence signal and to determine the level of protein expression. Image intensity analysis was performed on Image Lab software.

2.11. DC maturation after co-cultured with liposome-treated cancer cells

To assess the effects of liposomes on immune cells, D1 dendritic cells (DCs) were co-cultured with treated cancer cells in 96-well plates for 24 h. Thereafter, supernatants were collected and subjected to IL-12 measurement with an IL-12p40 sandwich ELISA kit (Biologen). D1DCs were harvested for FACS analysis. Cells were detached with PBS/EDTA (Sigma-Aldrich, St. Louis, USA), washed with FACS buffer and stained with the following antibodies: anti-CD11c-APC-eF780 (clone N418, Thermo Fisher Scientific), anti-CD40-APC (Clone 3/23, Biologen), anti-CD86-PE-cy7 (clone GL1, BD Biosciences), and anti-I-Ab (MHC class II; Clone M5/114.15.2, Thermo Fisher Scientific). DAPI was included for discrimination between living and dead cells. After staining for 30 min, cells were washed with FACS buffer to remove unbound antibodies and

resuspended in 100 µL FACS buffer. Flow cytometry was performed with an LSR-II cytometer (BD Biosciences) and data were analyzed using FlowJo (version 10).

2.12. Investigation of calreticulin exposure and High-mobility group box 1 secretion

Cells treated with chemotherapy were harvested and assessed for viability using DAPI staining and anti-mouse Alex Fluor647-labeled calreticulin (CRT) (Clone 1G6A7, Novus Biologicals, Englewood, USA). High-mobility group box 1 (HMGB1) protein release was also observed by immunofluorescence. MC38 and CT26 cells were fixed for 30 min using 4% paraformaldehyde and then permeabilized for 5 min using 0.5% Triton-X100 (Sigma-Aldrich) in PBS. The cells were incubated with 5 µg/ml anti-HMGB1 (Novus Biologicals) at 4 °C overnight and detected with an anti-rabbit AF488 (Invitrogen) at a 1:500 dilution. In all cases, starting cell number and media volume were controlled across both cell lines and all assays.

2.13. Colon cancer xenograft mouse model and assay of biodistribution in mice treated with different liposomes

An IR780-LP solution was prepared for observation of biodistribution. Female BABL/c mice (6–8 weeks) were subcutaneously inoculated with 1.5×10^5 CT26 cells on the right flank to establish the animal model. To investigate the drug biodistribution and tumor targeting efficacy *in vivo*, the tumor-bearing mice were randomly grouped ($n = 4$). When the tumor volume reached 200 mm^3 , mice were intravenously injected with free IR780 or IR780-LPs at 100 µg/kg of the IR780 dose. The mice were anesthetized with isoflurane at 1, 2, 4, 9, 12, 24, 48, and 72 h post-administration to monitor the real-time biodistribution by means of the IVIS Lumina system (PerkinElmer Inc., Waltham, MA, USA). After 72 h, the mice were sacrificed using CO₂. Major organs (heart, lung, liver, spleen, and kidney) and tumors were harvested for *ex vivo* imaging. Images were analyzed in Living Image 4.1 software (Caliper Life Sciences, USA) by defining a region of interest around the initial injection site that is then duplicated in all images.

2.14. Evaluation of antitumor effect and safety *in vivo*

To evaluate the antitumor efficacy and safety of the liposomes, 4×10^5 and 1×10^5 MC38 and CT26 cells in 100 µL PBS were subcutaneously injected into C57BL/6 and BALB/c mice, respectively. The mice were randomly divided into different groups ($n = 10$) on day 7 and intravenously injected with DTX (10 mg/kg) and PMX (15 mg/kg) every two days for five times, and subcutaneously injected with anti-PD-L1 (100 µg/mouse) every eight days for three times. The tumor volume and weight were measured every 2 days to observe the anti-tumor efficacy and toxicity *in vivo*. The tumor size was measured by using a caliper and tumor volumes were determined using the following formula: $V = L \times W \times H$ (L = the length; W = the width; and H = the height of the tumor). Survival time of the mice was analyzed using Kaplan-Meier survival curves.

2.15. Histology

Tumor tissues were harvested after treatment, followed by dehydration, embedding, and preparation of paraffine sections at 5 µm thickness. Tumor sections were then stained with Ki67 and hematoxylin and eosin (H&E), respectively, to visualize morphology and necrosis.

2.16. Blood analysis

To investigate the level of immune activation after treatment, immune cells (immune effector cells: CD4⁺, CD8⁺ T cells) and tumor-specific CD8+ T cells by MHC class I-peptide tetramer staining (Rpl18

and Adpgk) in the blood circulation of MC38 tumor-bearing mice were analyzed. Tumor-bearing mice were injected with different formulations via the tail vein. The presence of antigen-specific T lymphocytes was assessed by collecting 30 μ L blood via a caudal vein puncture on day 16 following the first treatment. The cells were stained with anti-CD4-FITC (Clone RM4-4 Thermo Fisher Scientific), anti-CD8-PE (Clone 53-6.7, eBioscience, Waltham, MA, USA), and anti-CD3-eFluor 450 after red blood cells were removed by lysis buffer (Clone 17A2, eBioscience). The APC-labeled Rpl18 tetramer and the PE-labeled Adpgk tetramer were then added to the staining mix. After being washed three times, the cells were analyzed using flow cytometry (Aurora, Cytek®, Amsterdam, The Netherlands) and the data was processed by FlowJo (version 10).

2.17. Statistical analysis

Data were presented as mean \pm standard deviation. One- and two-way analysis of variance was used when making multiple comparisons. Bonferroni posttests were performed when comparing all groups. A two-tailed Student's *t*-test was used when comparing two groups. *In vivo* tumor treatment studies were repeated in two independent experiments to ensure adequate sample size and reproducibility. All statistical analysis was performed using GraphPad Prism software 8.0 (La Jolla, CA, USA). Statistical significance was noted as follows: *, $p < 0.05$, **, $p < 0.01$, ***, $p < 0.001$, ****, $p < 0.0001$.

3. Results and discussion

3.1. Preparation and characterization of liposomes

With the aim to solve the problem of low solubility of DTX and increase the loading efficiency of PMX, liposomes were constructed based on our previous work [20]. The structures and physicochemical properties are shown in Fig. 2. From TEM photograph in Fig. 2A, we observed that the liposomes had a clear bilayer structure, round-shaped appearance, and a good dispersion, either with a single drug or co-load with both drugs. All liposomes were slightly negatively charged (~ -11 mV) due to the coating with PEG2000, which could be beneficial for reducing nonspecific binding, antibody opsonization, and hemolysis, together with a longer circulation time when used *in vivo* [25]. As indicated in Table S1, the diameters of DTX-loaded liposomes (DTX-LP) were 124 ± 6 nm with a polydispersity index (PDI) of 0.06 ± 0.01 and PMX-loaded liposomes (PMX-LP) were 128 ± 0.1 nm in diameter with PDI of 0.09 ± 0.01 . Co-loaded liposomes (DTX/PMX-LP) were 126 ± 3 nm in diameter with PDI of 0.09 ± 0.02 . The similar size of these different liposomes was consistent with the results from electron microscopy, which indicated that introducing another small molecule into the liposomes barely affected the physicochemical properties.

The encapsulation efficiency and drug loading of DTX and PMX were determined to further assess the quality of liposomes. As depicted in Table S2, the liposomes with DTX exhibited 95.6% encapsulation efficiency due to its high lipophilic capability, while the drug loading was 7.9%. However, the high entrapment of PMX was partially limited due to its inherent lipophobicity. By introducing cholesterol analog CHEMS,

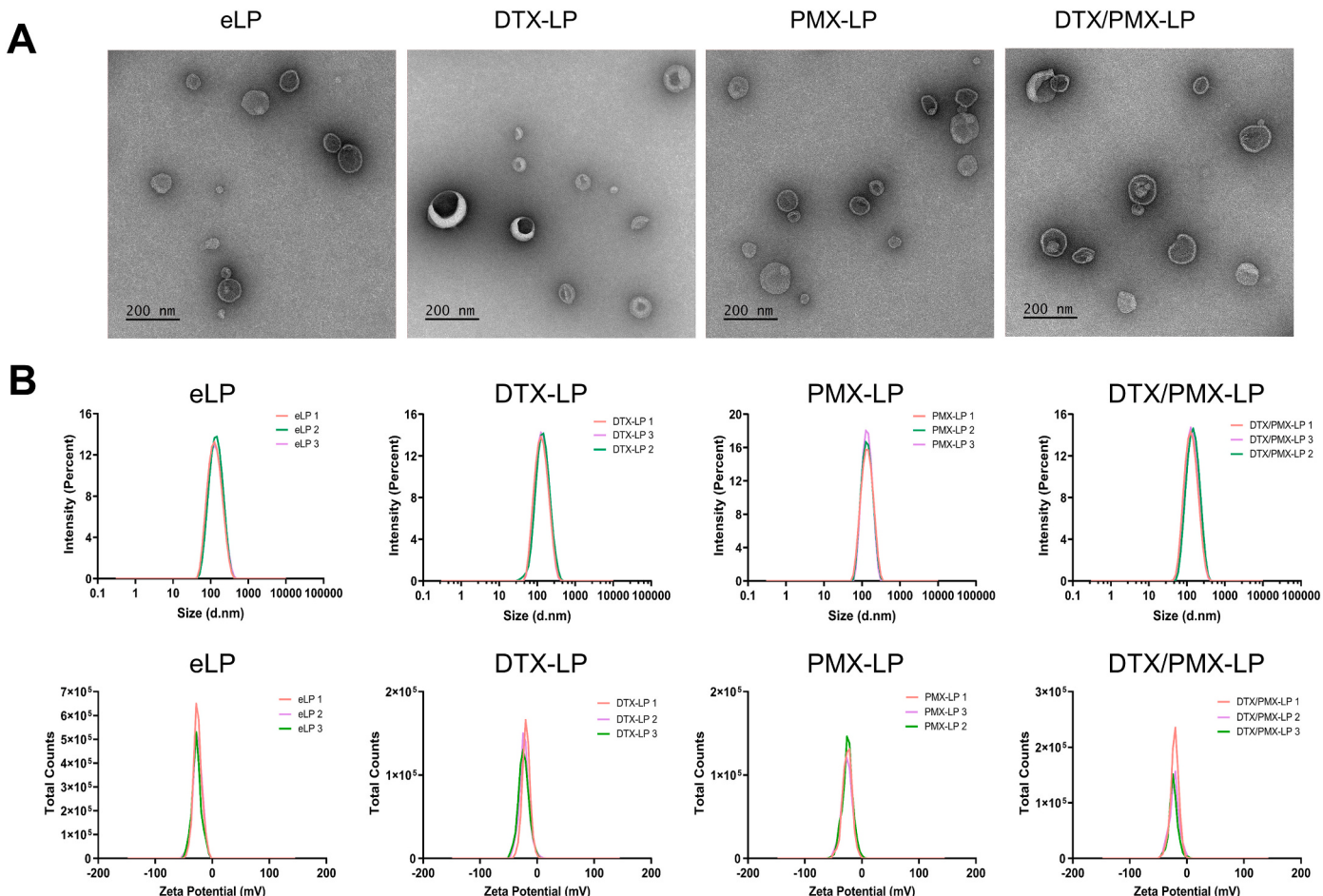


Fig. 2. Liposome characterization. A. The TEM photograph of liposomes. B. The size and zeta potential distribution of liposomes. Abbreviations: eLP: empty liposome; DTX-LP: DTX-loaded liposome; PMX-LP: PMX-loaded liposome; DTX/PMX-LP: co-loaded liposome.

liposome membranes tend to enlarge by enhancing the extent of hydration around the interfacial membrane region, which contributes to the entrapment of PMX. Furthermore, the research of Eldin and colleagues showed that the encapsulation efficiency decreased with an increasing dose of PMX [23]. For optimal efficacy, we chose 4 mg/ml of PMX as a desired hydration concentration. The final encapsulation efficiency and drug loading of PMX reached 14.2% and 10.9%, respectively.

3.2. Stability and release behavior of liposomes *in vitro*

Physicochemical stability under physiological conditions is very

important for nanoformulations, since they can influence the behaviors of nanoparticles *in vivo*. Therefore, we investigated the physicochemical stability of the prepared liposomes in PBS as well as in 10% and 50% serum. Following incubation with PBS (pH 7.4), the particle size and zeta potential of our liposomal formulations were similar to the initial status as shown in Fig. 3A. Similar results were obtained with liposomes incubated with serum (Fig. 3B). These liposomes exhibit stable structures in both 10% and 50% serum, which may facilitate the sustained release of the loaded drug *in vivo*. Notably, the stability was affected when liposomes were mixed with an acidic medium. The increasing diameter indicated that liposomes were sensitive to a low pH (Fig. 3A).

We also measured the drug release kinetics of our liposomes in PBS

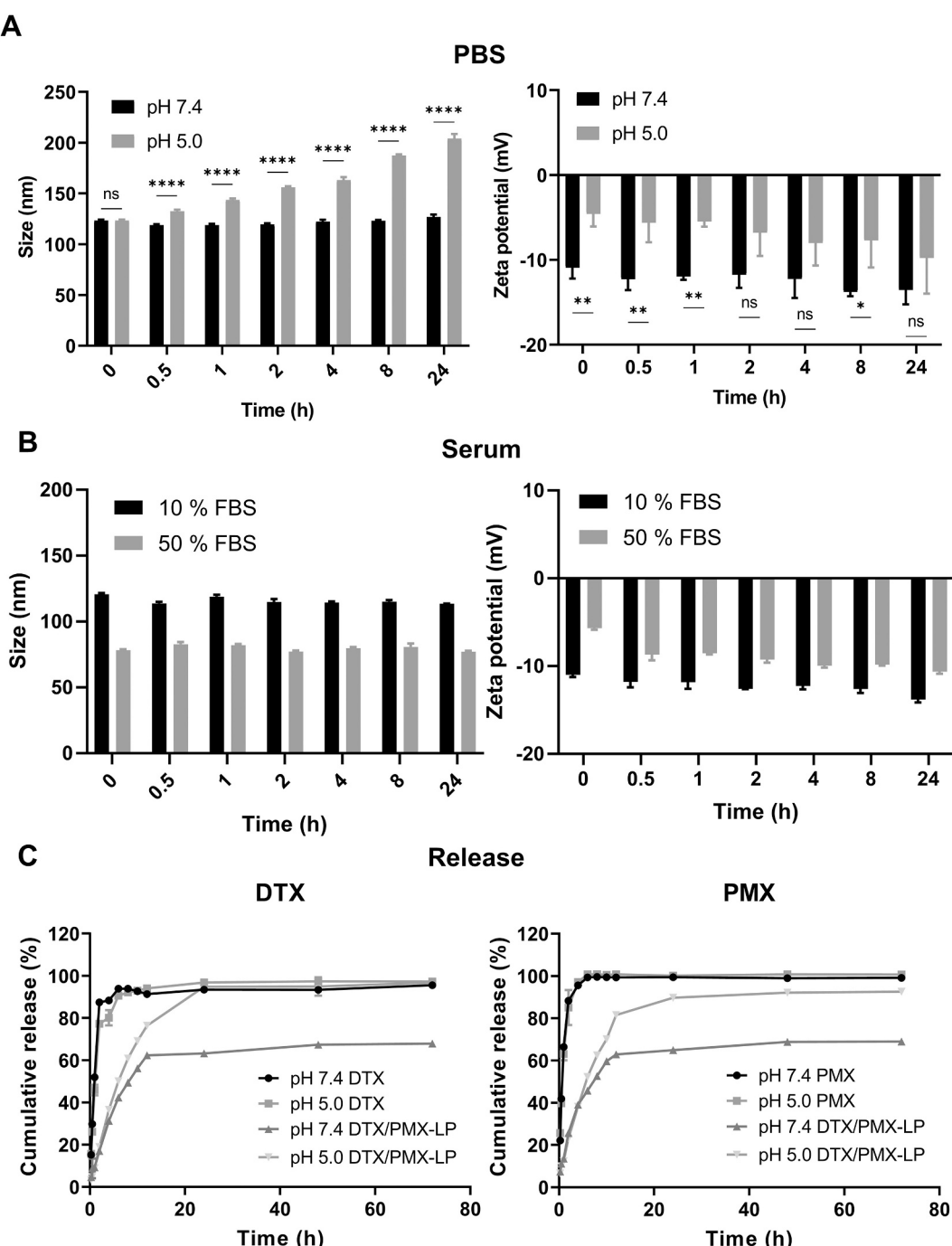


Fig. 3. Stability and release kinetics of liposomes. A. The stability of liposomes in PBS. B. The stability of liposomes in serum. C. The *in vitro* cumulative release behaviors of liposomes and free drugs.

with different pH at 37 °C in a thermo-shaker at a constant shaking velocity. The liposomes revealed a sustained release profile with different kinetics for each loaded drug, and release kinetics were pH-dependent (Fig. 3C). The cumulative release percentages of DTX and PMX in co-loaded liposomes were $68.0 \pm 0.1\%$ and $68.9 \pm 0.8\%$, respectively, in neutral environment (pH = 7.4) within 72 h. However, in acidic environment (pH = 5.0), the cumulative release percentages for DTX and PMX were 96.7 ± 1.6 and 92.6 ± 0.8 , respectively, within 72 h. These pH-sensitive liposomes can interact and induce endosomal membrane fusion or destabilization, allowing the encapsulated contents to be released efficiently into the cell cytoplasm [14]. Before being taken up by tumor cells, the liposomes could efficiently shelter cargos against the clearance in different ways, such as phagocytosis, enzymatic cleavage, or exclusion by detoxification [26]. Contrary to liposomes, there was no significant difference between both free drugs at pH 5.0 and pH 7.4 in PBS. Both free drugs exhibited much faster release than liposomes, reached to 100% within 12 h. The release behavior of free drugs also suggested that liposomes had a sustained-release effect. Our analysis indicated that pH-sensitive liposomes are well suited for efficient drug delivery into the cytoplasm and intracellular drug accumulation *in vitro*.

3.3. Evaluation of cellular internalization and retention

To determine whether our liposomes could bind to the cell membrane at low temperatures, cells were maintained at 4 °C during incubation. As shown in Fig. S1, the uptake difference between free IR780 and IR780-LP indicates stronger binding ability of liposomes. Furthermore, only dose-dependent responses were observed in both free dye and liposomes. The fluorescence in free IR780 did not change significantly with incubation time. However, liposomes could still induce stronger binding at a low temperature, *i.e.* 4 °C, compared to the free dye, which might be due to protein corona [27]. This protein corona is recognized by specialized receptors (over)expressed on the target cells, guiding the liposomes to their intended destination. If several separate epitopes from different corona proteins are exposed, each one may be identified by a different receptor, thereby facilitating liposomal drug uptake [27]. Liposomes made of anionic lipids tend to preferentially adsorb basic plasma proteins. For example, DOPE promotes the adsorption of apolipoproteins and serum albumin, while cholesterol induces the binding of complement proteins [28].

Since both DTX and PMX exert intracellular biological effects, the uptake ability of liposomes were evaluated in MC38 and CT26 cells using an encapsulated fluorescent dye. After incubation with free IR780 or IR780-LPs, both cell lines exhibited time- and dose-dependent responses (Fig. 4A). The fluorescence intensity of IR780 was gradually increased under higher doses and longer periods. There was significantly more uptake of liposomes compared to the free drug, even when the concentration of IR780 reached a plateau at 16 µg/mL. Meanwhile, fluorescence microscopy was used to visualize the internalization of liposomes (Fig. 4B). These results indicated that liposomes were located within the cytoplasm and showed stronger fluorescent signals under longer drug exposure, which was in accordance with our FACS data. In general, drug accumulation of nano-formulations is higher than that of free drugs. This might attribute to different mechanisms for small molecules and nanoparticles when entering cells [29]. Normally small molecules, such as IR780, can enter into the cytoplasm through passive diffusion, while liposomes enter into cells *via* receptor-mediated internalization (*i.e.* clathrin) [30]. Our liposomal delivery system provides a promising possibility for enhancing the biological effects of drugs, especially those with low lipophilicity.

Furthermore, we assessed whether liposomes could provide extended drug retention at the site of interest. To this end, after removal of excess IR780 or IR780-LPs, cells were washed thoroughly and examined for their ability of retention under different conditions. As seen in Fig. 4C, both MC38 and CT26 cells moderately preserved their ability to retain IR780. However, a stronger signal was retained from our

liposomes in comparison to free drug, which underlined the high retention ability of liposomes.

3.4. Cytotoxicity assay of liposomal formulations *in vitro*

After confirming the ability of cellular uptake, the formulations were carefully tested for safety and cytotoxicity using MTS assays. First, cells were incubated with empty liposomes (no drug encapsulated) and their viability was determined. As displayed in Fig. S2, nearly no cytotoxicity was observed in MC38 or CT26 cells treated with empty liposomes at concentrations ranging from 0.003 to 300 µg/mL after 24 or 48 h. However, after 72 h and at concentrations between 0.03 and 300 µg/mL, MC38 cells exhibited a slight, but not significant, decrease in viability. After 72 h of incubation, CT26 did not exhibit any influence on cell viability by our empty liposomes. This indicates the liposomes had good biocompatibility and low cytotoxicity, which was the prerequisite for safe conduct of the follow-up experiments with our liposomes. For drug-loaded liposomes, all the liposome groups showed significantly stronger cell inhibition than the corresponding free drugs in both cell lines after 48 h and 72 h of incubation (Fig. 5A). When exposed to higher concentrations and over longer periods, the anti-proliferation rate of cells was substantially decreased, demonstrating a good correlation between toxicity and time/dose in MC38 and CT26 cells. For MC38 cells, the IC₅₀ after 48 h of incubation with free DTX, free PMX, and free DTX + PMX were approximately 1.365 µg/mL, 1.37 µg/mL, and 0.024 µg/mL, respectively. The IC₅₀ of DTX-LPs, PMX-LPs, and DTX/PMX-LPs were 0.12 µg/mL, 0.024 µg/mL, and 0.01 µg/mL, which showed 11.4-fold, 357.1-fold, and 2.4-fold increased cytotoxicity, respectively, compared to the corresponding IC₅₀ of the free drugs. Similar results were obtained in CT26 cells, where the IC₅₀ of our liposomes was 22.6-fold, 32.3-fold, and 5-fold lower than free drugs. These results supported the hypothesis that liposomal delivery of these drugs induced a stronger tumor inhibition activity.

In order to further evaluate the therapeutic effects induced by drug-loaded liposomes, we measured Annexin V-PI signals to detect cell death directly. As a typical apoptosis marker, Annexin V is exposed in the process of cell apoptosis. As illustrated in Fig. 5B, a significantly greater number of MC38 and CT26 cells underwent apoptosis 24 h after liposomal treatment, especially early apoptosis. The empty liposome barely induced apoptosis, which is consistent with our MTS results. DTX-LPs, PMX-LPs, and DTX/PMX-LPs led to higher apoptosis rates ($72.8 \pm 3.3\%$, $65.4 \pm 7.5\%$, and $76.6 \pm 2.7\%$, respectively) in MC38 cells than free drugs: DTX ($3.1 \pm 5\%$), PMX ($23.9 \pm 2.8\%$), and DTX + PMX ($33.3 \pm 3.6\%$). As mentioned before, the liposomal formulations displayed higher efficiency of cellular internalization and retention than free drugs, which led to more drug accumulation in the cytoplasm of the cancer cells. As a result, we observed a rise in the amount of intracellular DTX and PMX, consequently inducing stronger apoptotic cascade. In addition, the larger difference between the free combination and our co-loaded liposomes (Fig. 5B & Fig. S3&4) might come from the use of different detection methods. Based on the aforementioned data, we hereby shed light on liposomes as a promising drug delivery system, which strengthened the molecules' capacity to reach their pharmacological target and improve the performance of chemotherapeutic agents.

3.5. Thymidylate synthase (TS) expression in colon tumor lines

It has been reported that chemosensitivity of PMX is linked to the levels of TS expression—higher expression of TS is correlated with lower sensitivity to PMX. In non-small cell lung cancer, it has been demonstrated that DTX is able to suppress TS expression, leading to a higher sensitivity to PMX. To determine whether DTX could increase the sensitivity to PMX in colorectal cancer, we measured the level of TS protein expression on MC38 and CT26 cells after docetaxel exposure by means of western blot. Various doses of docetaxel were added to both

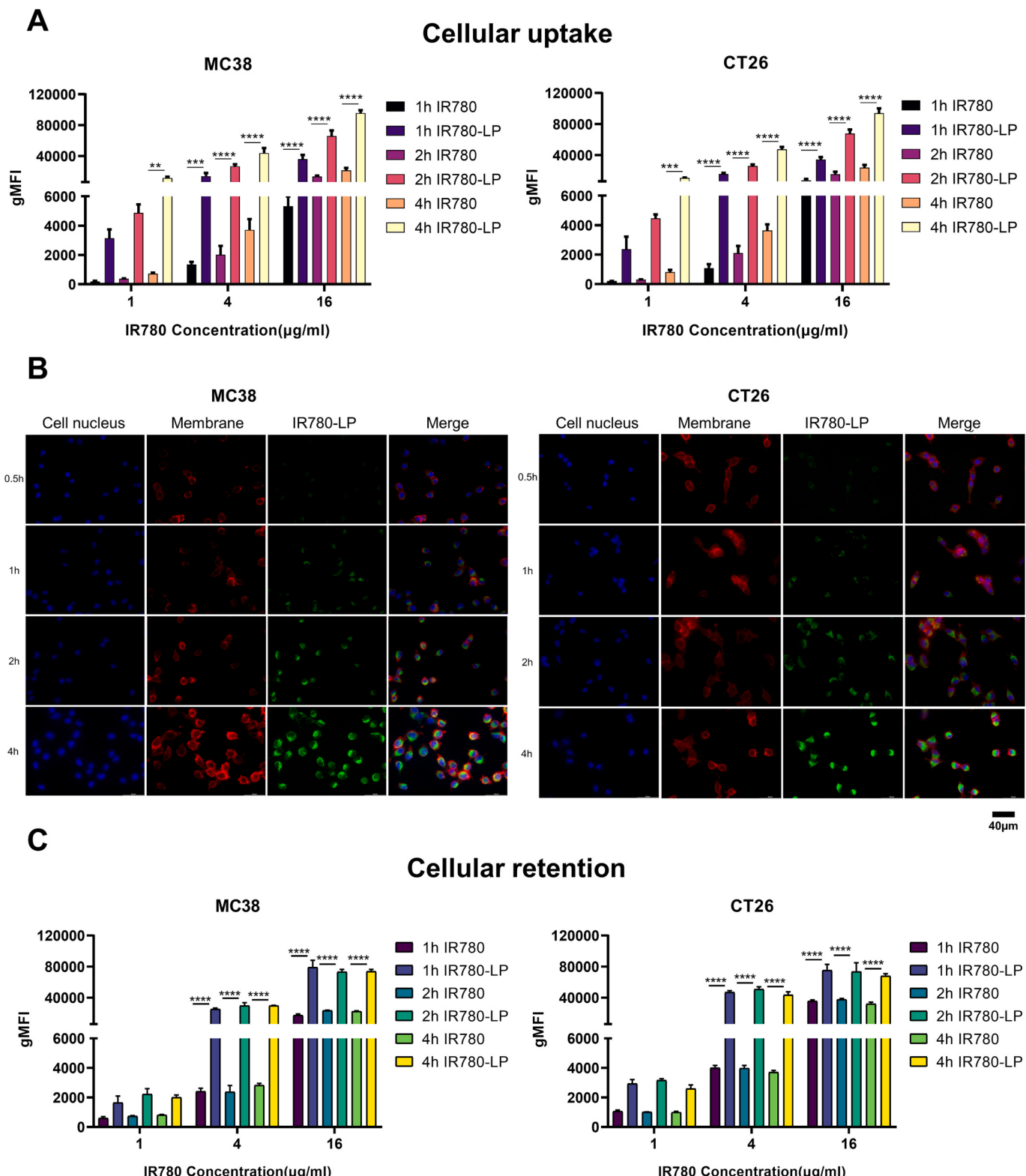


Fig. 4. Liposomal uptake and retention characteristics. A. Intracellular uptake ability of 1, 4 and 16 μg/ml formulations at 37 °C for 1, 2 or 4 h. B. Fluorescence pictures of cellular uptake after incubation with liposomes for 0.5, 1, 2, and 4 h. Cell nuclei were stained with DAPI (blue) and cell membranes were stained with anti-CD44-PE (red). The IR780 signal is depicted in green ($n = 3$, scale bar is 40 μm). C. The retention ability of cells at different time points and drug concentrations at 4 °C. After a 4-h incubation, formulations were withdrawn, cells were washed with PBS, and fresh medium was added. (gMFI: Geometric mean fluorescence intensity). (For interpretation of the references to colour in this figure legend, the reader is referred to the web version of this article.)

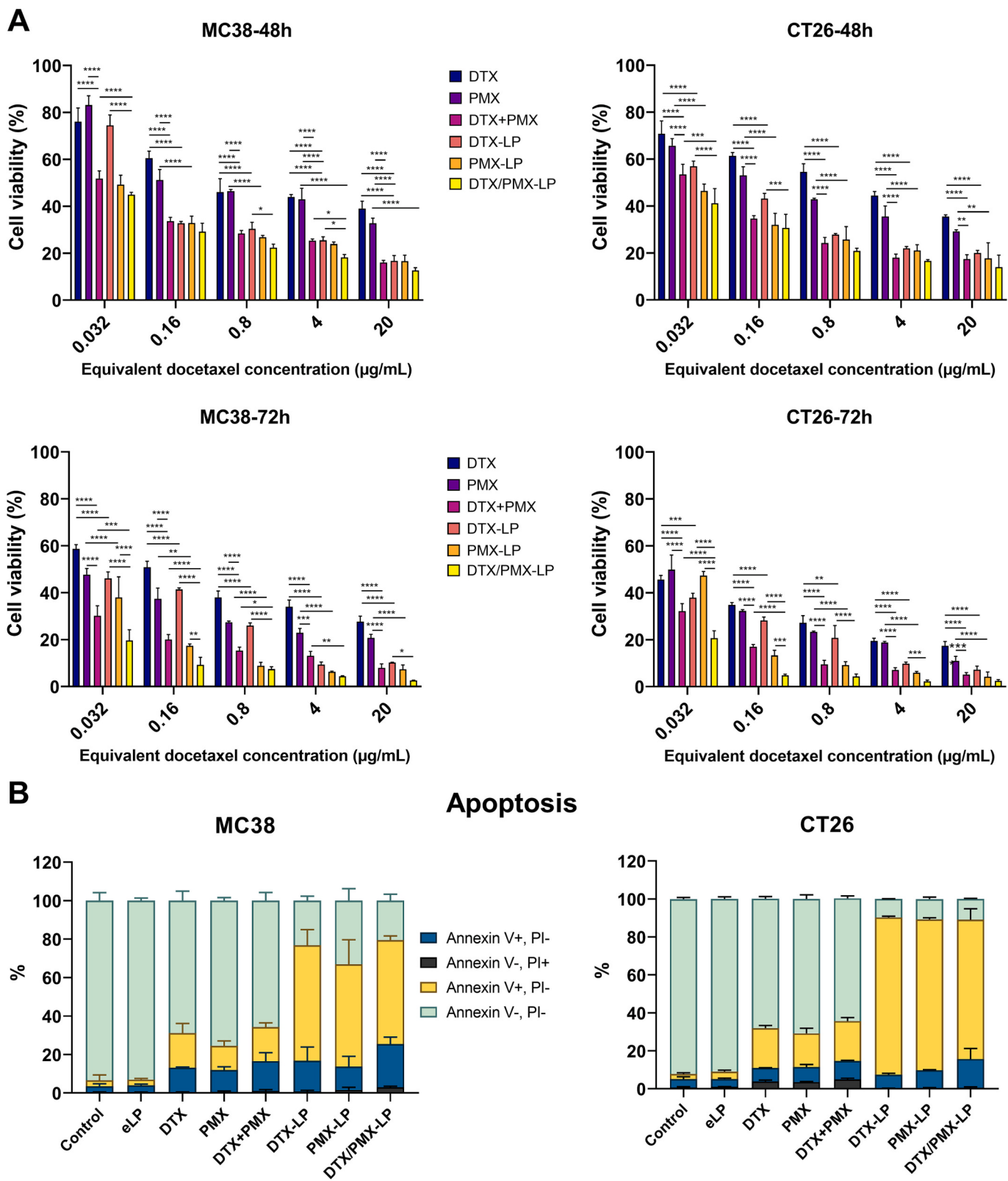


Fig. 5. Cytotoxicity of liposomes *in vitro*. A. Cell viability of MC38 and CT26 cells after incubation with DTX, PMX, DTX + PMX, DTX-LPs, PMX-LPs, and DTX/PMX-LPs for 48 and 72 h ($n = 4$, equivalent PMX concentration is 0.048, 0.16, 1.2, 6, 30 $\mu\text{g}/\text{mL}$). B. The apoptotic rate after treatment with different combinations of drugs and formulations ($n = 3$, results were shown in mean \pm S.D., *, $p < 0.05$, **, $p < 0.01$, and ***, $p < 0.001$).

cell types and the results showed that docetaxel indeed influenced TS expression in a dose-dependent manner (Fig. 6). At higher concentrations of docetaxel, cancer cells downregulated TS expression. According to our data, this inhibition of TS expression was beneficial for high pemetrexed sensitivity, which in line with our hypothesis to combine docetaxel with pemetrexed.

3.6. DC maturation after co-cultured with liposome-treated colon cancer cells

Cancer cells release various cues and antigens during the process of tumor growth. Released antigens can be presented by the major histocompatibility complex (MHC) class II molecules or cross-presented into the MHC class I molecules on DCs that migrate from the tumor site to draining lymph nodes to initiate T cell activation [31]. Successful DC maturation is the prerequisite for subsequent stimulation of T cells. During this maturation process, upregulated costimulatory molecules (such as CD40, CD80, and CD86) and release of pro-inflammatory cytokines (such as IL12) can be observed when specific cues (e.g., damage-associated molecular patterns) are presented. Based on this knowledge, we co-cultured MC38 and CT26 cancer cells, which had been treated with liposomes, with dendritic cells and investigated DC maturation markers. For both MC38 and CT26 cells, an increase of MHC II and, to a lesser extent, MHC I on DCs was detected (Fig. 7). Cancer cells treated with the liposomes induced the highest upregulation of DC maturation markers (i.e., CD40, CD80, and CD86) compared to untreated cells. Both MC38 and CT26 cell types that were pre-treated with DTX/PMX-LP induced strong IL12 secretion from DCs. However, the IL12 secretion more pronounced when co-incubated with CT26 cells, which indicates that, in comparison to free drugs, liposomes could enhance the activation of DCs more efficiently in the CT26 model. In contrast, surface expression of CD40, CD80, and CD86 on DCs, that were co-cultured with untreated cancer cells, was similar to those of DCs cultured alone (no co-culture). Thus, DTX/PMX-LP-treated cancer cells induced DC maturation *in vitro*, which resulted in highly activated DCs with could potentially enhance proliferation and activation of T lymphocytes *in vivo*.

3.7. CRT exposure and HMGB1 secretion

It has been reported that some specific chemotherapeutic agents,

such as paclitaxel and doxorubicin, can induce a favorable form of apoptosis, so-called ICD in the tumor microenvironment [32]. The dying cancer cells can then act as a vaccine to trigger tumor-specific immune responses, due to the release of cancer-associated antigens and the secretion of specific cues, such as immune activation of damage-associated molecular patterns [33]. Typically, some of these cues, such as the pre-apoptosis exposure of CRT (transport from the endoplasmic reticulum), and HMGB1, are potent signals for antigen-presenting cells [34,35]. They can stimulate and induce the maturation of DCs and promote the release of pro-inflammatory cytokines, such as IL12, which further regulate T cell polarization and activate anti-tumor immune responses [36]. Therefore, we sought to explore the underlying mechanism behind our phenotype by testing CRT exposure and HMGB1 secretion after treatment in the two colon cancer cell models. After 24 h of incubation with free drugs or liposomes, cells were stained with FITC-labeled anti-CRT and measured by means of flow cytometry. The chemotherapeutic agents, whether alone or in combination, induced high CRT expression compared to the negative control group (Fig. 8A&B). Among all groups, DTX/PMX-LPs exhibited the highest induction of CRT on both MC38 and CT26 cells, which explains its great capacity for DC maturation as shown before. Additionally, through immunofluorescence staining against HMGB1, we found that treatment of CT26 cells with DTX + PMX and DTX/PMX-LPs induced the transport of HMGB1 from the cell nuclei to the cytoplasm (Fig. 8C). Furthermore, the nuclear export of HMGB1 contributes to the ICD of the apoptotic cancer cells, which was induced by the cytotoxic drugs and our liposomal formulations. Similar activity was observed in MC38 cells (Fig. 8D). Taken together, DTX/PMX-LPs induced high CRT exposure and HMGB1 secretion in both cell lines, suggesting the ability of our formulation to induce ICD, which can lead to robust anti-tumor immune responses.

3.8. Biodistribution of liposomes on CT26 tumor-bearing mice *in vivo*

The specific drug distribution and accumulation in the site of interest directly influences the therapeutic efficacy as well as side effects. Due to the high tissue penetration ability of the near-infrared fluorescence of IR780, the real-time biodistribution could be monitored noninvasively. By making use of this advantage, we detected the specific accumulation of the IR780 signal at the tumor sites of CT26 tumor-bearing mice after

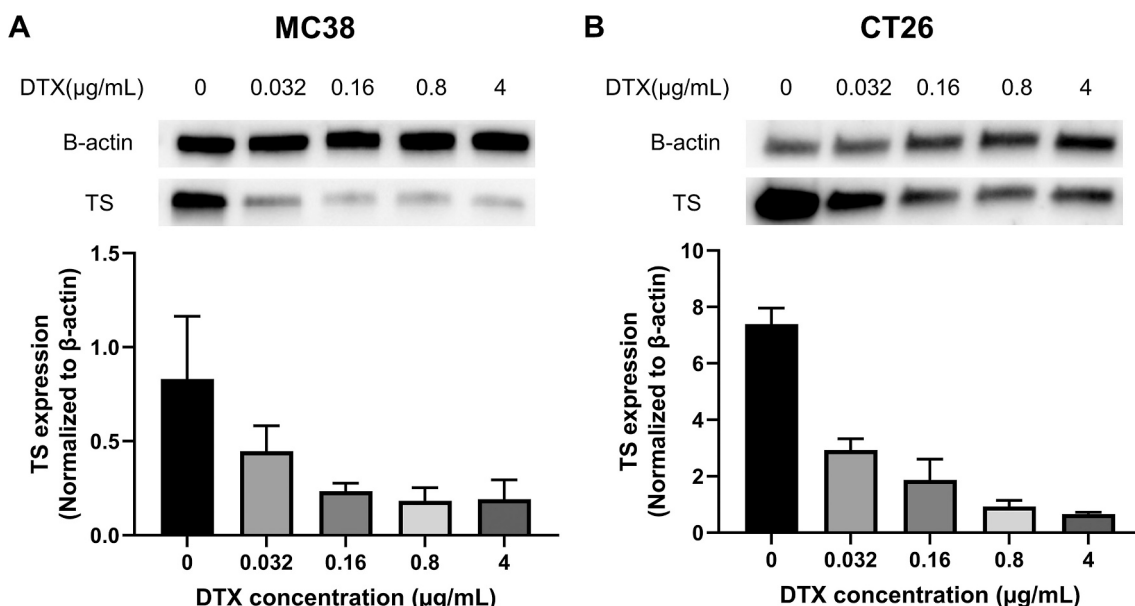


Fig. 6. TS expression on CT26 & MC38 cells. Cell lysates were collected after incubated with DTX for 24 h. Dose-dependence of DTX in TS expression MC38 (A) & CT26 (B) were characterized by western blot analyses.

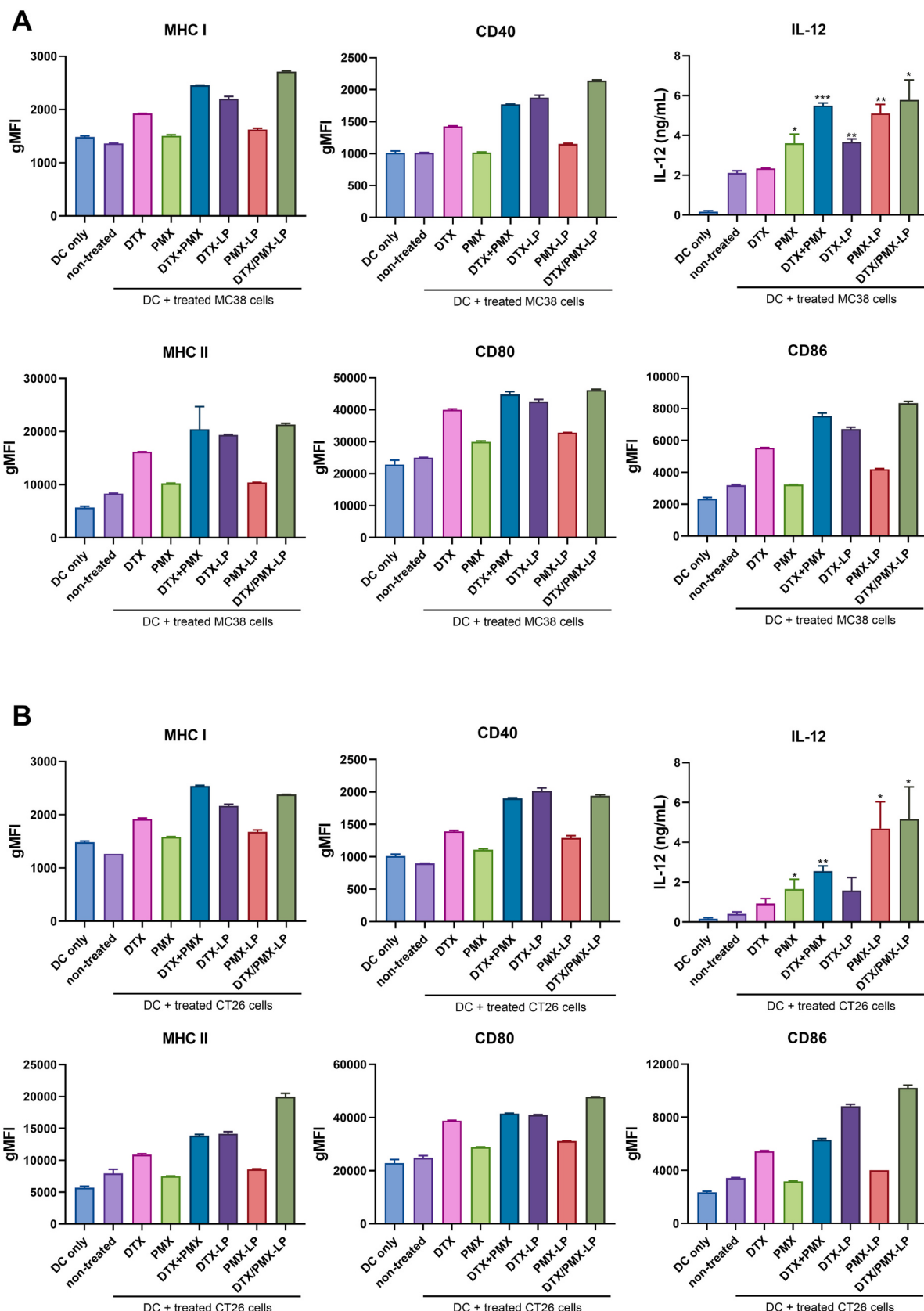


Fig. 7. DC maturation after incubation with liposome-treated, apoptotic tumor cells *in vitro*. A. DC maturation after co-cultured with treated MC38 cells. B. DC maturation after co-culture with treated CT26 cells.

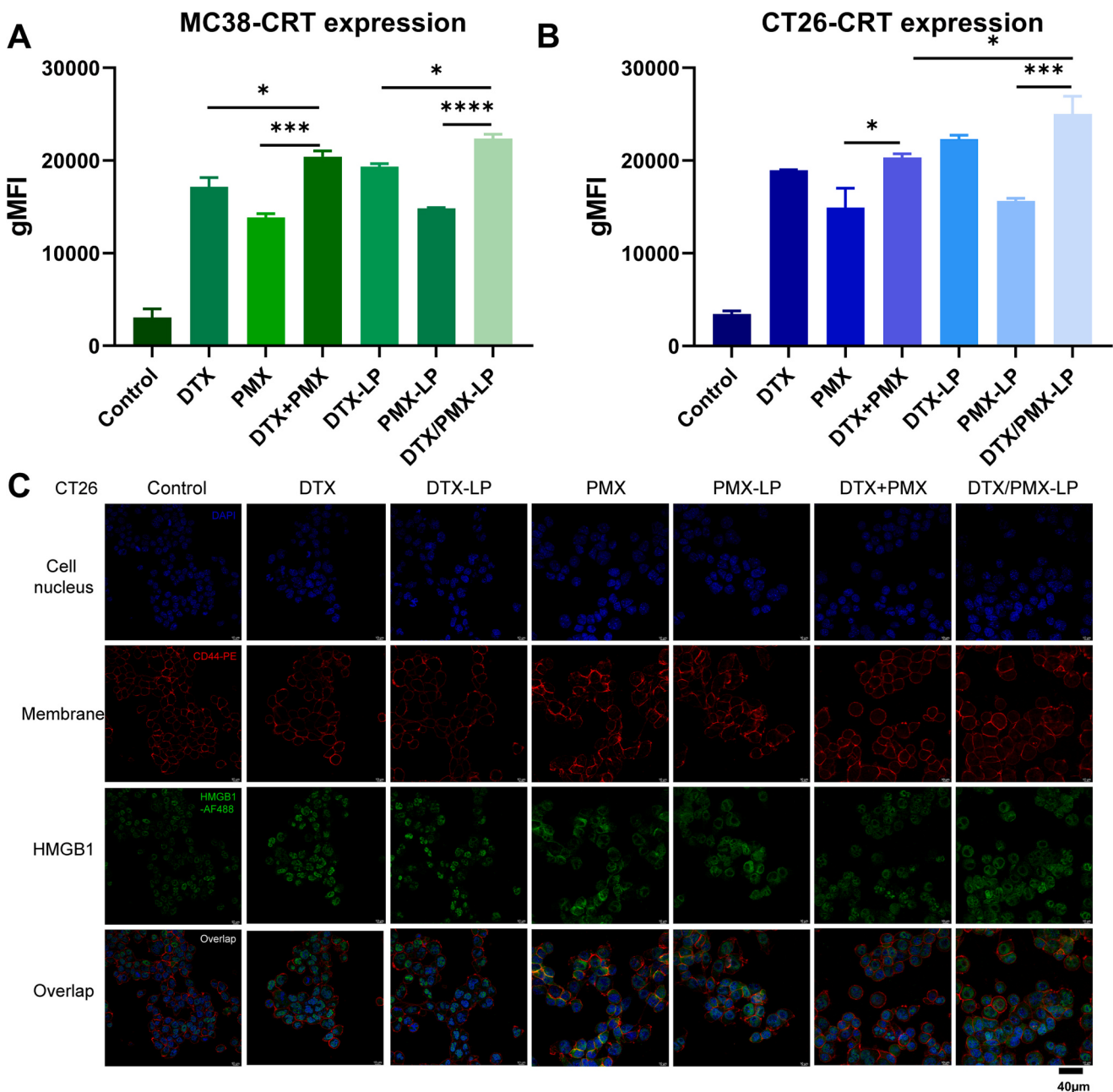


Fig. 8. In vitro CRT exposure and HMGB1 secretion after incubation with drugs and liposomes. A. The CRT expression of MC38 cells after treatments. B. The CRT expression of CT26 cells after treatments. C. The fluorescence photographs of HMGB1 secretion on CT26 cells, scale bar are 40 μ m. ($n = 3$, results were shown in mean \pm S.D., *, $p < 0.05$, **, $p < 0.01$, and ****, $p < 0.0001$).

intravenous injection of free IR780 or IR780-LPs captured with the IVIS near-infrared imaging system. As a result, the IR780 fluorescence signal could be observed as early as 1 h after injection, and the signals of free IR780 and IR780-LPs gradually increased at the tumor site until 24 h (Fig. 9A). After 24 h, free IR780 was constantly eliminated and exhibited reduced accumulation at the tumor site. In contrast, the fluorescence signal detected in the IR780-LPs group remained high even at 72 h after injection *in vivo* and *ex vivo* (Fig. 9A&9B), which is likely due to the property of liposomes to maintain in the blood circulation for an extended period of time. It is known that the reticuloendothelial system (RES) can rapidly clear nanoparticles from systemic circulation, preventing their retention at target sites. The PEGylated liposomes tended to display less aggregation, opsonization, and phagocytosis [37], which prolonged their circulation time and strongly reduce the number of required injections. The tumor accumulation of IR780-LPs was higher

than that of free IR780 at each time point (Fig. 9C), and the reason may be that liposomes passively targeted tumors due to the enhanced permeability and retention effect of tumor tissue [38]. We observed that the biodistribution of free IR780 in the liver and spleen was lower than that of IR780-LPs, which might also be due to the long circulation ability of liposomes (Fig. 9D). These results have shown that the signal of IR780-LPs was 3.48-fold higher than that of free IR780 in the tumor, which indicates that our liposomes are likely more efficient at targeting and treating tumors and thereby potentially limiting off-target toxicity. Taken together, these results show that the liposomes we prepared exhibited a potent targeting ability and long circulation ability, which warranted an investigation of the treatment efficacy.

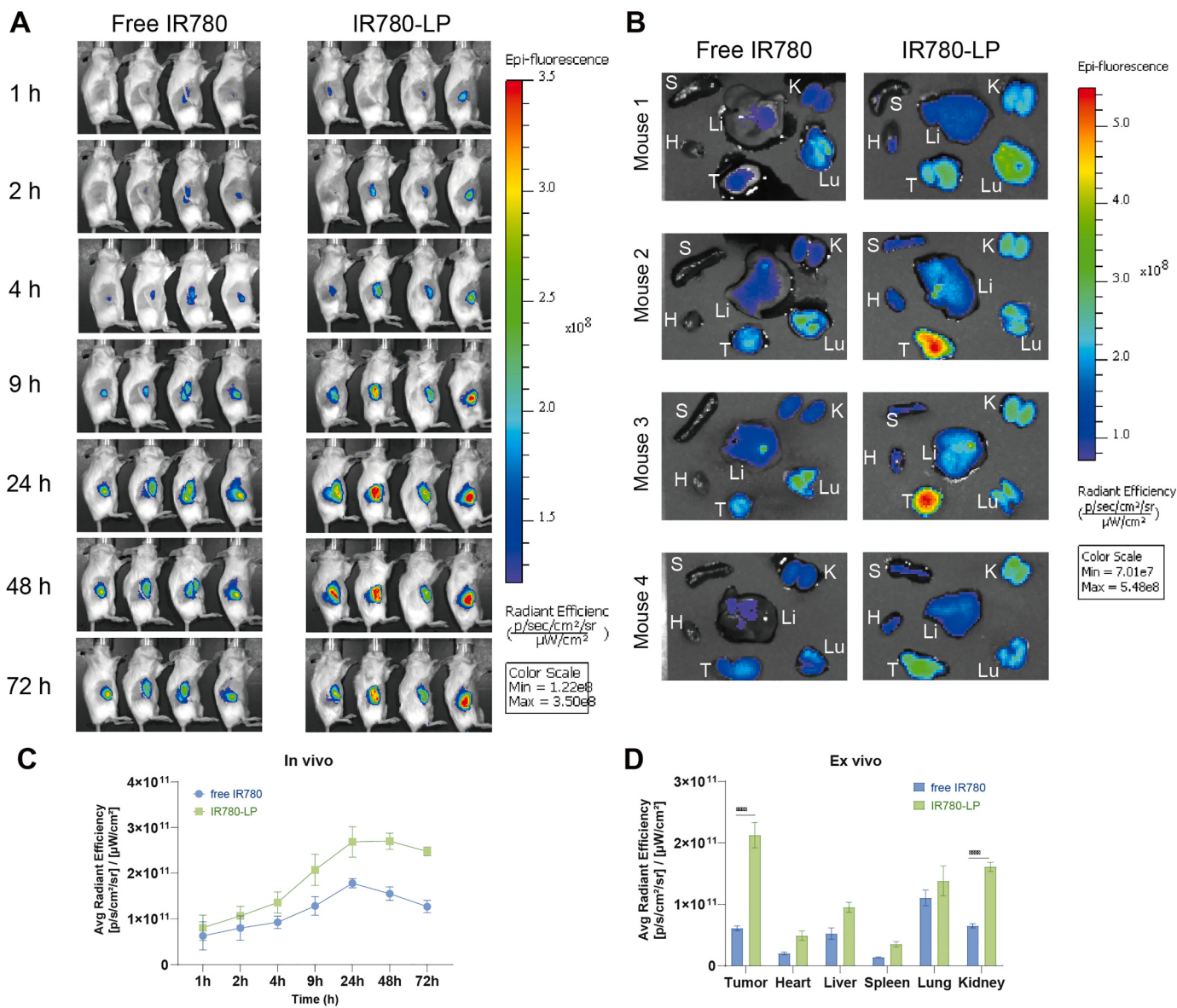


Fig. 9. Representative biodistribution in CT26 tumor-bearing mice *in vivo* and *ex vivo*. A. 1, 2, 4, 9, 24, 48, and 72 h after intravenous injection of free IR780 or IR780-LPs. B. The *ex vivo* fluorescence imaging of major organs and tumors at 72 h post-injection. C. Mean fluorescence intensity (MFI) values of hearts (H), livers (Li), spleens (S), lungs (Lu), kidneys (K), and tumors (T) at 48 h post-injection ($n = 4$, results were shown in mean \pm S.D., ****, $p < 0.0001$).

3.9. Antitumor efficacy *in vivo*

To evaluate the antitumor efficacy of the liposomal formulations, we subcutaneously injected CT26 and MC38 colon tumor cells in BALB/c and C57BL/6 mice, respectively. For each model, a total of 60 tumor-bearing mice were randomly divided into 6 groups for intravenous injections of the following agents: 1) control group with saline injection, 2) DTX injection, 3) DTX + PMX injection, 4) anti-PD-L1 injection, 5) DTX/PMX-LP injection, 6) DTX/PMX-LP plus anti-PD-L1 injection. The administration frequency and dose are indicated in Fig. 9A. Considering the introduction of anti-PD-L1 in the studies, we examined PD-L1 expression on both MC38 and CT26 cells by flow cytometry before starting animal experiment. Our results suggested that both cell lines expressed a high level of PD-L1 after overnight intervention with IFN- γ (Fig. S5), which paved a path to our rationale for combining anti-PD-L1 with the chemotherapeutic 1 agents.

Traditional chemotherapy introduces severe adverse effects, which obstruct the clinical application of chemotherapy. We observed weight loss in all groups of MC38 tumor-bearing mice that received the free

drugs, whereas the body weights of the mice in the groups receiving liposomes remained basically unchanged or slightly increased, similar to the control group (Fig. 10I). Such effects were more pronounced in CT26 tumor-bearing mice, which showed dramatic weight loss during treatment with the free drugs (Fig. 10E). Nevertheless, mice receiving DTX/PMX-LPs or DTX/PMX-LPs combined with anti-PD-L1 displayed alleviated tumor burden, which can be attributed to the passively targeting ability of our liposomes (Fig. 10D&H).

As indicated in Fig. 10H, MC38 tumor-bearing mice initially responded to all the treatments. Among these treatments, the combination of DTX/PMX-LPs with anti-PD-L1 exhibited the greatest statistically significant therapeutic effect: over 80% of the mice got complete remission of the tumor (Fig. 10F&G). Although pronounced tumor inhibition was found when applying the free drug combination (DTX + PMX) or anti-PD-L1 alone, the introduction of our liposomes exhibited significantly superior effects on tumor regression. Unlike MC38 tumors, the CT 26 tumors showed negligible response to anti-PD-L1 therapy (Fig. 10D). The anti-PD-L1 therapy resistance was reversed when combined with chemotherapeutic agents, which may be due to the combined

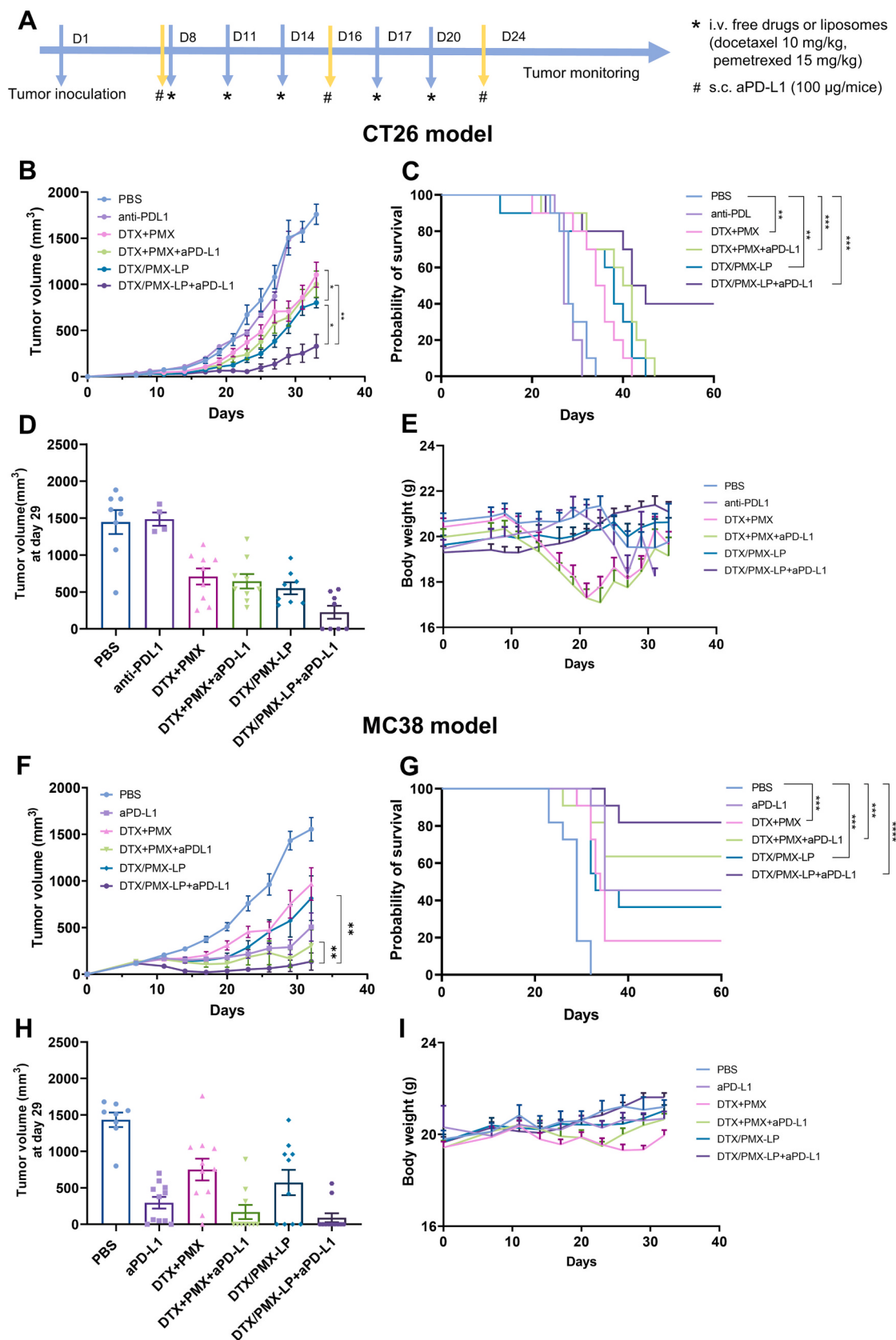


Fig. 10. In vivo therapeutic efficacy of liposomes against subcutaneous CT26 and MC38 tumors. A. The therapeutic schedule of treatments. Free DTX + PMX and DTX/PMX-LPs were injected intravenously, and anti-PD-L1 was injected subcutaneously. B. The tumor growth curves of CT26 tumor-bearing mice. C. Survival rates of CT26 tumor-bearing mice. D. The tumor size at day 29 after CT26 tumor inoculation. E. The body weight changes of CT26 tumor-bearing mice. F. The tumor growth curves of MC38 tumor-bearing mice. G. Survival rates of MC38 tumor-bearing mice. H. The tumor size at day 29 after MC38 tumor inoculation. I. The body weight changes of MC38 tumor-bearing mice ($n = 10$, results were shown in mean \pm S.D., *, $p < 0.05$, **, $p < 0.01$, and ***, $p < 0.001$).

activity of ICD. However, only the combination of DTX/PMX-LPs with anti-PD-L1 treatment was able to completely eliminate the tumors (Fig. 10C). Notably, when co-loaded into liposomes, DTX/PMX-LPs gained a stronger therapeutic effect in comparison to the free DTX + PMX (Fig. 10B&D) when anti-PD-L1 is involved, which supported our hypothesis that liposomes could lead to high drug accumulation at the tumor sites and boost the anti-tumor immunity *via* induction of ICD. In addition, the liposome-based combination (DTX/PMX-LPs + anti-PD-L1) had a better therapeutic effect on the inhibition of tumor growth than the free DTX + PMX, which was consistent with our results of high drug retention in tumor tissue when using liposomes as shown previously. To further illustrate the anti-tumor efficiency at the histological level, we collected tumor tissue and prepared pathological slices for morphology and necrosis investigation. As indicated in Fig. S7, the lowest proliferation rate was found in the liposome-based combination group, while free combination showed moderate tumor inhibition. Besides, a large number of necrotic tumor cells were observed in the group treated with liposome-based combination (Fig. S8), which was consistent with our above-mentioned results. Owing to the synergistic effect of anti-PD-L1 with DTX/PMX-LP, the co-treatment was able to effectively inhibit tumor growth and delay tumor progression and significantly increase the survival rate of mice bearing these lethal tumors.

3.10. Neoepitope-specific circulating T cells

As appealing targets for therapeutic cancer vaccines, neoepitopes have been gaining more attention since they are not subject to the central immune tolerance and are not expressed in healthy tissues [39]. To control tumor growth, neoepitopes, which are released by dying tumor cells, are presented to naive T cells by APCs for priming and activation. Activated neoepitope-specific CD8⁺ T cells then leave the lymph node, enter the tumor tissue, and exert antitumor activities. Some chemotherapy types were reported to promote the exposure of (neo) epitopes, facilitating cancer-specific immune responses, as an *in situ* ‘vaccine’ [40]. To explore whether liposome-based chemotherapy combined with immunotherapy could also augment cancer-specific immune responses, we examined the levels of circulating lymphocytes in the blood of treated mice at day 16 after the first treatment of MC38 tumor-bearing mice and analyzed specific cell markers by means of flow cytometry. Firstly, we noticed that the percentages of CD3⁺ and CD8⁺ T cells were significantly increased in the blood of mice treated with the combination of DTX/PMX-LPs and anti-PD-L1 (Fig. 11A&C). At the same time, animals treated with DTX/PMX-LPs plus anti-PD-L1 had a lower average number of CD4⁺ T cells in their blood than mice treated with the free DTX + PMX, but this difference was not statistically significant (Fig. 11B). These findings demonstrated our liposomes are suitable as a modality to enhance cancer-specific immune responses.

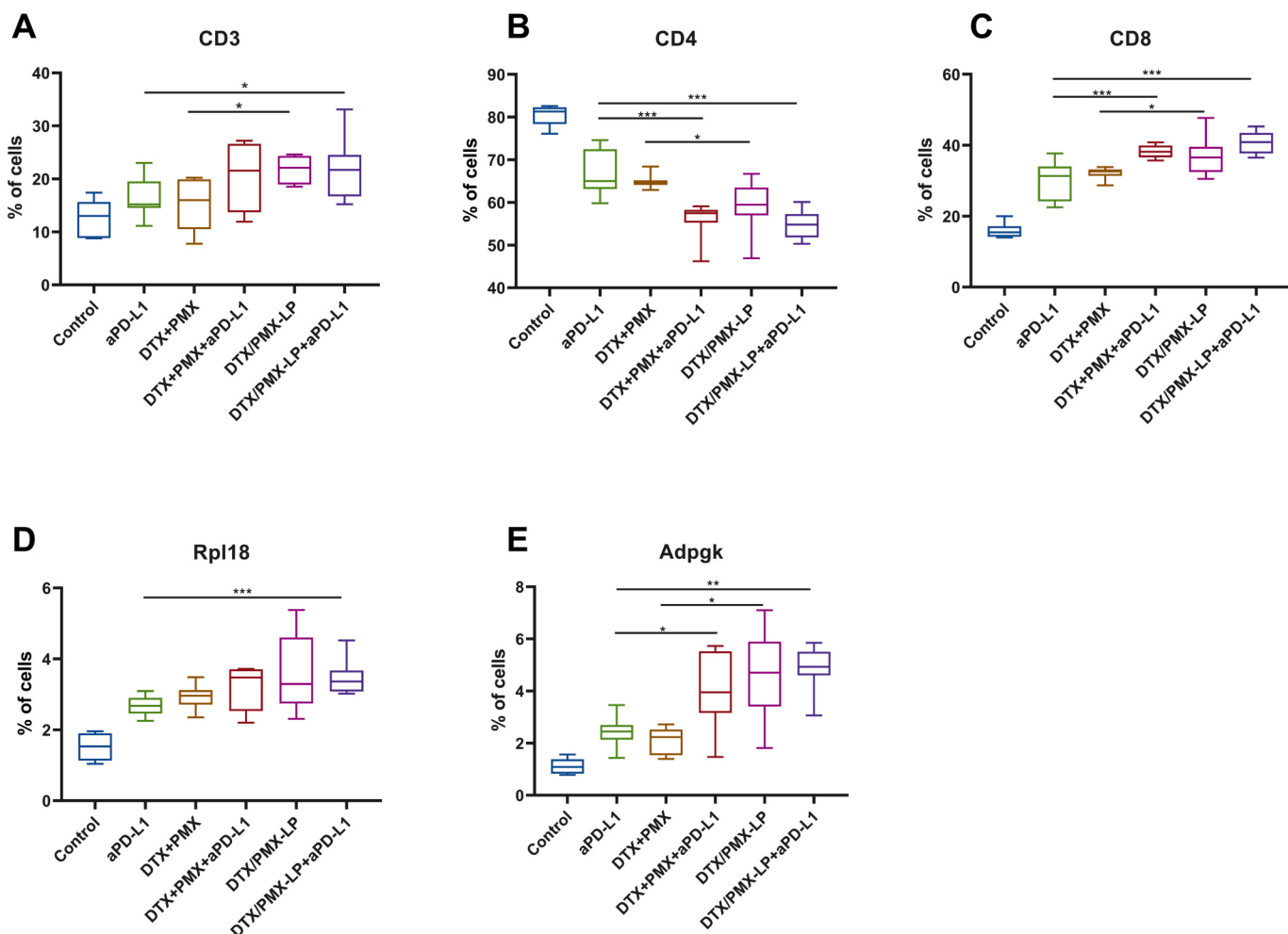


Fig. 11. The levels of circulating CD3⁺, CD4⁺, CD8⁺, and MC38 neoepitope-specific CD8⁺ T cells. A. The percentages of CD3⁺ T cells collected from the blood of mice on day 26. B. The percentages of CD3⁺CD4⁺ T cells collected from the blood of mice on day 26. C. The percentages of CD3⁺CD8⁺ T cells collected from the blood of mice on day 26. D. The percentages of Rpl18⁺ CD8⁺ T cells collected from the blood of mice on day 26. E. The percentages of Adpgk⁺ CD8⁺ T cells collected from the blood of mice on day 26 ($n = 8$, results were shown in mean \pm S.D., * $p < 0.05$, ** $p < 0.01$, and *** $p < 0.001$).

It has been reported that dominant CD8⁺ T cell immune responses toward neoepitopes can be triggered by mutated peptide epitopes in the ribosomal protein L18 (Rpl18) and ADP-dependent glucokinase (Adpgk) in the murine MC38 colorectal cancer model [41]. To our knowledge, the capacity of liposome-mediated chemotherapy to operate as an *in-situ* vaccination has not been demonstrated for cancer neoepitopes (Rpl18 and Adpgk). As shown in Fig. 11D&E, in contrast to the free DTX + PMX or anti-PD-L1 alone, DTX/PMX-LPs resulted in a considerable increase of MC38 neoepitope-specific (both Rpl18 & Adpgk) CD8⁺ T cells. The results indicate that the DTX/PMX-LP plus anti-PD-L1 enhanced high levels of MC38 neoepitope-specific CD8⁺ T cells in the blood circulation. Thus, these effects are better, compared to those observed for either the free DTX + PMX or DTX/PMX-LP. It has been reported that high levels of circulating T cells were primed in MC38 cancer model after combining chemotherapeutic agents with immunotherapy [42]. Here, our results show strongly elevated blood levels of such T cells after the combination of DTX/PMX-LPs with anti-PD-L1, thereby providing proof to the *in-situ* vaccination ability of liposome-mediated chemoimmunotherapy. Hence, liposome-mediated chemoimmunotherapy exerted a strong cancer-specific immune response in mice bearing MC38 tumors.

4. Conclusion

Strategies to improve the treatment of cancer can rely on enhancing the direct tumor-killing ability of cytostatic drugs or boosting immune responses via specific methods to activate the immune system. Although boosting immune responses through methods such as therapeutic antibodies or vaccines are very promising, efficient treatments are needed to improve the induction of direct (immunogenic) cell death of cancer cells. At the same time an effective anti-cancer immune response must be generated in absence of systemic toxicity. In this study, we analyzed if liposome-mediated chemoimmunotherapy could improve the tumor-killing ability of immune T cells by chemo-sensitizing cancer cells toward PMX with DTX. We aimed to induce strong ICD while also inhibiting cancer immune resistance with anti-PD-L1 co-therapy. We demonstrated that PMX/DTX liposomes possessed good physicochemical properties and therapeutic effects both *in vitro* and *in vivo*. Cellular internalization studies *in vitro* and biodistribution analysis *in vivo* demonstrated that liposomes could be passively targeted to the tumor sites, high level of therapeutic drug could be retained, and therefore decreased off-target toxicity. Based on anti-tumor studies *in vivo*, we could show that liposome-mediated chemoimmunotherapy had the greatest therapeutic efficacy and even achieved complete remission in mice bearing either MC38 or CT26 colorectal cancer. Furthermore, this combination increased the number of (neo)antigen-specific T cells in the blood. Overall, we show that our pH-sensitive liposomal platform for co-loading of DTX and PMX has great clinical potential and offers a well-controlled release vehicle for combining chemotherapy with diverse immunotherapies.

Author contribution

Conceptualization, Z.G.; methodology, Z.G., C.G.D.S., L.J.C. and F.O.; Original data collection and analysis, or interpretation — Z.G.; writing - original draft preparation — Z.G.; writing - review and editing—Z.G., C.G.D.S., Y.H., Q.L., T.S., K.M.; visualization, — Z.G., T.S., R.K.; supervision— C.G.D.S., F.O. and L.J.C.; Final additions—L.J.C. All authors contributed to the article and approved the submitted version.

CRediT author statement

Zili Gu: Conceptualization, Data curation, Writing- Original draft preparation, Visualization, Investigation. **Candido da Silva:** Methodology, Writing- Reviewing and Editing, Supervision. **Yang Hao:** Investigation, Validation. **Timo Schomann:** Visualization, Writing-

Reviewing and Editing. **Marcel G.M. Camps:** Investigation. **Koen van der Maaden:** Validation. **Qi Liu:** Methodology, Writing- Reviewing and Editing. **Roman I. Koning:** Visualization. **Erik Bos:** Visualization. **Ferry Ossendorp:** Writing- Reviewing and Editing, Supervision. **Luis J. Cruz:** Supervision.

Declaration of Competing Interest

The authors declare no conflicts of interest. The funders had no role in the design of the study; in the collection, analyses, or interpretation of data; in the writing of the manuscript; or in the decision to publish the results.

Data availability

No data was used for the research described in the article.

Acknowledgments

This project has received funding from the European Union's Horizon 2020 research and innovation programme under the Marie Skłodowska Curie grant agreement No 777682 (CANCER), 734684 (CHARMED), PRISAR2 (872860); ACORN (807281), SIMICA (852985), 952520 (BIOSAFETY). 861190 (PAVE), 857894 (CAST), 859908 (NOVAMRI), 956477 (PIANO). Timo Schomann received funding from the European Commission grants H2020-MSCA-RISE CANCER (777682) and H2020-WIDESPREAD-05-2017-Twinning SIMICA (852985).

Appendix A. Supplementary data

Supplementary data to this article can be found online at <https://doi.org/10.1016/j.jconrel.2022.11.049>.

References

- [1] J. Shi, P.W. Kantoff, R. Wooster, O.C. Farokhzad, Cancer nanomedicine: progress, challenges and opportunities, *Nat. Rev. Cancer* 17 (2017) 20–37, <https://doi.org/10.1038/nrc.2016.108>.
- [2] C.G. Da Silva, F. Rueda, C.W. Löwik, F. Ossendorp, L.J. Cruz, Combinatorial prospects of nano-targeted chemoimmunotherapy, *Biomaterials* 83 (2016) 308–320, <https://doi.org/10.1016/j.biomaterials.2016.01.006>.
- [3] Jacqueline B. Stone, Lisa M. DeAngelis, Cancer treatment-induced neurotoxicity: a focus on newer treatments, *Nat. Rev. Clin. Oncol.* 13 (2016) 92–105, <https://doi.org/10.1002/aur.1474.Replication>.
- [4] K.A. Whitehead, R. Langer, D.G. Anderson, Knocking down barriers: advances in siRNA delivery, *Nat. Rev. Drug Discov.* 8 (2009) 129–138, <https://doi.org/10.1038/nrd2742>.
- [5] P.G. Corrie, Cytotoxic chemotherapy: clinical aspects, *Medicine (Baltimore)* 36 (2007) 24–28, <https://doi.org/10.1016/j.mpmed.2007.10.012>.
- [6] W. John, J. Picus, C.D. Blanke, J.W. Clark, L.N. Schulman, E.K. Rowinsky, D. E. Thornton, P.J. Loehrer, Activity of multitargeted antifolate (Pemetrexed disodium, LY231514) in patients with advanced colorectal carcinoma: results from a phase II study, *Cancer* 88 (2000) 1807–1813, [https://doi.org/10.1002/\(SICI\)1097-0142\(20000415\)88:8<1807::AID-CNCR8>3.0.CO;2-L](https://doi.org/10.1002/(SICI)1097-0142(20000415)88:8<1807::AID-CNCR8>3.0.CO;2-L).
- [7] J. Sigmund, H.H.J. Backus, D. Wouters, O.H. Temmink, G. Jansen, G.J. Peters, Induction of resistance to the multitargeted antifolate Pemetrexed (ALIMTA) in WiDr human colon cancer cells is associated with thymidylate synthase overexpression, *Biochem. Pharmacol.* 66 (2003) 431–438, [https://doi.org/10.1016/S0006-2952\(03\)00287-9](https://doi.org/10.1016/S0006-2952(03)00287-9).
- [8] D.C. Christoph, B.R. Asuncion, B. Hassan, C. Tran, J.D. Maltzman, D. J. O'Shannessy, M.W. Wynes, T.C. Gauler, J. Wohlschlaeger, M. Hoiczyk, M. Schuler, W.E. Eberhardt, F.R. Hirsch, Significance of folate receptor alpha and thymidylate synthase protein expression in patients with non-small-cell lung cancer treated with pemetrexed, *J. Thorac. Oncol.* 8 (2013) 19–30, <https://doi.org/10.1097/JTO.0b013e31827628ff>.
- [9] A.R. Hanauske, U. Eismann, O. Oberschmidt, H. Pospisil, S. Hoffmann, H. Hanauske-Abel, D. Ma, V. Chen, P. Paoletti, C. Niyikiza, In vitro chemosensitivity of freshly explanted tumor cells to pemetrexed is correlated with target gene expression, *Investig. New Drugs* 25 (2007) 417–423, <https://doi.org/10.1007/s10637-007-9060-9>.
- [10] A.H. Kyle, L.A. Huxham, D.M. Yeoman, A.I. Minchinton, Cancer Therapy : Preclinical Limited Tissue Penetration of Taxanes : A Mechanism for Resistance in Solid Tumors 13, 2007, pp. 2804–2811.

- [11] D. Landesman-Milo, D. Peer, Altering the immune response with lipid-based nanoparticles, *J. Control. Release* 161 (2012) 600–608, <https://doi.org/10.1016/j.jconrel.2011.12.034>.
- [12] J. Shi, A.R. Votruba, O.C. Farokhzad, R. Langer, Nanotechnology in drug delivery and tissue engineering: from discovery to applications, *Nano Lett.* 10 (2010) 3223–3230, <https://doi.org/10.1021/nl102184c>.
- [13] K. Shao, S. Singha, X. Clemente-Casares, S. Tsai, Y. Yang, P. Santamaria, Nanoparticle-based immunotherapy for cancer, *ACS Nano* 9 (2015) 16–30, <https://doi.org/10.1021/nm5062029>.
- [14] S.R. Paliwal, R. Paliwal, S.P. Vyas, A review of mechanistic insight and application of pH-sensitive liposomes in drug delivery, *Drug Deliv.* 22 (2015) 231–242, <https://doi.org/10.3109/10717544.2014.882469>.
- [15] R.S. Herbst, D. Morgenstern, C. Boshoff, The biology and management of non-small cell lung cancer, *Nature* 553 (2018) 446–454, <https://doi.org/10.1038/nature25183>.
- [16] L. Zitvogel, O. Kepp, G. Kroemer, Immune parameters affecting the efficacy of chemotherapeutic regimens, *Nat. Rev. Clin. Oncol.* 8 (2011) 151–160, <https://doi.org/10.1038/nrclinonc.2010.223>.
- [17] L.A. Emens, Chemoimmunotherapy: reengineering tumor immunity, *Cancer Princ. Pract. Oncol. Annu. Adv. Oncol.* 2 (2012) 203–216, <https://doi.org/10.1007/s00262-012-1388-0.Chemoimmunotherapy>.
- [18] S. Shen, H.J. Li, K.G. Chen, Y.C. Wang, X.Z. Yang, Z.X. Lian, J.Z. Du, J. Wang, Spatial targeting of tumor-associated macrophages and tumor cells with a pH-sensitive cluster nanocarrier for cancer chemoimmunotherapy, *Nano Lett.* 17 (2017) 3822–3829, <https://doi.org/10.1021/acs.nanolett.7b01193>.
- [19] I.H. Lee, S. An, M.K. Yu, H.K. Kwon, S.H. Im, S. Jon, Targeted chemoimmunotherapy using drug-loaded aptamer-dendrimer bioconjugates, *J. Control. Release* 155 (2011) 435–441, <https://doi.org/10.1016/j.jconrel.2011.05.025>.
- [20] Z. Gu, Q. Wang, Y. Shi, Y. Huang, J. Zhang, X. Zhang, G. Lin, Nanotechnology-mediated immunochemotherapy combined with docetaxel and PD-L1 antibody increase therapeutic effects and decrease systemic toxicity, *J. Control. Release* 286 (2018) 369–380, <https://doi.org/10.1016/j.jconrel.2018.08.011>.
- [21] D.A. Schaefer, S. Geeganage, N. Amaladas, Z.H. Lu, E.R. Rasmussen, A. Sonyi, D. Chin, A. Capen, Y. Li, C.M. Meyer, B.D. Jones, X. Huang, S. Luo, C. Carpenito, K. D. Roth, A. Nikolayev, B. Tan, M. Brahmachary, K. Chodavarapu, F.C. Dorsey, J. R. Manro, T.N. Doman, G.P. Donoho, D. Surguladze, G.E. Hall, M. Kalos, R. Novosadly, The folate pathway inhibitor pemetrexed pleiotropically enhances effects of cancer immunotherapy, *Clin. Cancer Res.* 25 (2019) 7175–7188, <https://doi.org/10.1158/1078-0432.CCR-19-0433>.
- [22] C. Conte, F. Ungaro, G. Maglio, P. Tirino, G. Siracusano, M.T. Sciortino, N. Leone, G. Palma, A. Barbieri, C. Arra, A. Mazzaglia, F. Quaglia, Biodegradable core-shell nanoassemblies for the delivery of docetaxel and Zn (II)-phthalocyanine inspired by combination therapy for cancer, *J. Control. Release* 167 (2013) 40–52, <https://doi.org/10.1016/j.jconrel.2012.12.026>.
- [23] N.E. Eldin, H.M. Elnahas, M.A.E. Mahdy, T. Ishida, Liposomal pemetrexed: formulation, characterization and in vitro cytotoxicity studies for effective management of malignant pleural mesothelioma, *Biol. Pharm. Bull.* 38 (2015) 461–469, <https://doi.org/10.1248/bpb.b14-00769>.
- [24] Y. Fan, Q. Wang, G. Lin, Y. Shi, Z. Gu, T. Ding, Combination of using prodrug-modified cationic liposome nanocomplexes and a potentiating strategy via targeted co-delivery of gemcitabine and docetaxel for CD44-overexpressed triple negative breast cancer therapy, *Acta Biomater.* 62 (2017) 257–272, <https://doi.org/10.1016/j.actbio.2017.08.034>.
- [25] A. Venault, K.J. Hsu, L.C. Yeh, A. Chinnathambi, H.T. Ho, Y. Chang, Surface charge-bias impact of amine-contained pseudowzwitterionic biointerfaces on the human blood compatibility, *Colloids Surf. B: Biointerfaces* 151 (2017) 372–383, <https://doi.org/10.1016/j.colsurfb.2016.12.040>.
- [26] S. Lewicki, M. Lesniak, E.K. Machaj, M. Antos-Bielska, E.A. Trafny, J. Kocik, Z. Pojda, Physical properties and biological interactions of liposomes developed as a drug carrier in the field of regenerative medicine, *J. Liposome Res.* 27 (2017) 90–98, <https://doi.org/10.3109/08982104.2016.1166510>.
- [27] G. Caracciolo, Liposome-protein corona in a physiological environment: challenges and opportunities for targeted delivery of nanomedicines, *nanomedicine nanotechnology, Biol. Med.* 11 (2015) 543–557, <https://doi.org/10.1016/j.nano.2014.11.003>.
- [28] A.L. Capriotti, G. Caracciolo, G. Caruso, P. Foglia, D. Pozzi, R. Samperi, A. Laganà, DNA affects the composition of lipoplex protein corona: a proteomics approach, *Proteomics* 11 (2011) 3349–3358, <https://doi.org/10.1002/pmic.201000803>.
- [29] R. Mo, Q. Sun, N. Li, C. Zhang, Intracellular delivery and antitumor effects of pH-sensitive liposomes based on zwitterionic oligopeptide lipids, *Biomaterials* 34 (2013) 2773–2786, <https://doi.org/10.1016/j.biomaterials.2013.01.030>.
- [30] D. Montizaan, K. Yang, C. Reker-Smit, A. Salvati, Comparison of the uptake mechanisms of zwitterionic and negatively charged liposomes by HeLa cells, *nanomedicine nanotechnology, Biol. Med.* 30 (2020), 102300, <https://doi.org/10.1016/j.nano.2020.102300>.
- [31] R.M. Steinman, I. Mellman, Immunotherapy: bewitched, bothered, and bewildered no more, *Science* (80-) 305 (2004) 197–200, <https://doi.org/10.1126/science.1099688>.
- [32] X. Duan, C. Chan, W. Lin, Nanoparticle-mediated immunogenic cell death enables and potentiates cancer immunotherapy, *Angew. Chem. Int. Ed.* 58 (2019) 670–680, <https://doi.org/10.1002/anie.201804882>.
- [33] G. Kroemer, L. Galluzzi, O. Kepp, L. Zitvogel, Immunogenic cell death in cancer therapy, *Annu. Rev. Immunol.* 31 (2013) 51–72, <https://doi.org/10.1146/annurev-immunol-032712-100008>.
- [34] M. Michaud, I. Martins, A.Q. Sukkurwala, S. Adjemian, Y. Ma, P. Pellegatti, S. Shen, O. Kepp, M. Scoazec, G. Mignot, S. Rello-Varona, M. Tailler, L. Menger, E. Vacchelli, L. Galluzzi, F. Ghiringhelli, F. Di Virgilio, L. Zitvogel, G. Kroemer, Autophagy-dependent anticancer immune responses induced by chemotherapeutic agents in mice, *Science* (80-) 334 (2011) 1573–1577, <https://doi.org/10.1126/science.1208347>.
- [35] L. Zitvogel, O. Kepp, L. Senovilla, L. Menger, N. Chaput, G. Kroemer, Immunogenic tumor cell death for optimal anticancer therapy: the calreticulin exposure pathway, *Clin. Cancer Res.* 16 (2010) 3100–3104, <https://doi.org/10.1158/1078-0432.CCR-09-2891>.
- [36] D.V. Krysko, A.D. Garg, A. Kaczmarek, O. Krysko, P. Agostinis, P. Vandenberghe, Immunogenic cell death and DAMPs in cancer therapy, *Nat. Rev. Cancer* 12 (2012) 860–875, <https://doi.org/10.1038/nrc3380>.
- [37] J.S. Suk, Q. Xu, N. Kim, J. Hanes, L.M. Ensign, PEGylation as a strategy for improving nanoparticle-based drug and gene delivery, *Adv. Drug Deliv. Rev.* 99 (2016) 28–51, <https://doi.org/10.1016/j.addr.2015.09.012>.
- [38] K. Maruyama, Intracellular targeting delivery of liposomal drugs to solid tumors based on EPR effects, *Adv. Drug Deliv. Rev.* 63 (2011) 161–169, <https://doi.org/10.1016/j.addr.2010.09.003>.
- [39] F. Lang, B. Schrörs, M. Löwer, Ö. Türeci, U. Sahin, Identification of neoantigens for individualized therapeutic cancer vaccines, *Nat. Rev. Drug Discov.* 21 (2022) 261–282, <https://doi.org/10.1038/s41573-021-00387-y>.
- [40] M.F. Pichon, M. Labroquère, K. Rezaï, F. Lokiec, Variations of soluble Fas and cytokeratin 18-Asp 396 neo-epitope in different cancers during chemotherapy, *Anticancer Res.* 26 (2006) 2387–2392.
- [41] B.J. Hos, M.G.M. Camps, J. van den Bulk, E. Tondini, T.C. va den Ende, D. Ruano, K. Franken, G.M.C. Janssen, A. Ru, D.V. Filippov, R. Arens, P.A. van Veelen, N. Miranda, F. Ossendorp, Identification of a neo-epitope dominating endogenous CD8 T cell responses to MC-38 colorectal cancer, *Oncoinmunology* 9 (2020), <https://doi.org/10.1080/2162402X.2019.1673125>.
- [42] C.G. Da Silva, M.G.M. Camps, T.M.W.Y. Li, L. Zerrillo, C.W. Löwik, F. Ossendorp, L. J. Cruz, Effective chemoimmunotherapy by co-delivery of doxorubicin and immune adjuvants in biodegradable nanoparticles, *Theranostics*. 9 (2019) 6485–6500, <https://doi.org/10.7150/thno.34429>.